Spectrum of Engineering Sciences
ISSN (e) 3007-3138 (p) 3007-312X Volume 4, Issue 5, 2026

INTELLIGENT PREDICTIVE MODELING OF FERROHYDRODYNAMIC FLOW OVER A ROTATING DISC USING NEURAL NETWORKS AND RANDOM FOREST ALGORITHMS

[1]Muhammad Jebran Khan, [*2]Muhammad Sohail, [3]Muhammad Fawad, [4]Junaid Ullah Jan, [5]Muhammad Asfandyar

[1-5]Department of Computing and Technology, Sarhad University, Peshawar, 25000, Khyber Pakhtunkhwa, Pakistan

[1]jibran.csit@suit.edu.pk, [*2]sohail.csit@suit.edu.pk, [3]Fawadkhattak585@gmail.com, [4]Junaidullahjan5@gmail.com , [5]asfand5454@gmail.com

DOI:-

Keywords
Ferrofluid Dynamics, Rotating Disc Flow, Heat Transfer Optimization, New Iterative Method (NIM), Machine Learning Predictive Models

Article History
Received: 15 April 2026
Accepted: 17 May 2026
Published: 20 May2026

Corresponding Author: *

Muhammad Sohail

Abstract

The study in this paper explores the dynamic behavior of ferrofluids over a rotating disc and identifies the key parameters including the effect of the thermal Rayleigh number, ferrohydrodynamic effect and volume fraction of nanoparticles on the velocity, temperature and concentration profiles. These intricate relationships were deciphered and accurate predictive models were developed using a novel approach that integrated the New Iterative Method (NIM) with cutting-edge machine learning algorithms such as neural networks and Random Forest models. The results reveal a strong interaction between thermal and hydrodynamic parameters, which indicates that the heat transfer and flow characteristics can be significantly improved by optimizing these parameters. Such applications as thermal management, energy systems, and industrial cooling require precision and efficiency, having far-reaching implications. The predictive models generated in this work demonstrated a high accuracy level, which was confirmed by the good agreement obtained with experimental data for different velocity and temperature conditions. There is very little difference between the predicted and measured values, which highlights reliability and strength of the approach. The findings of this study contribute to the understanding of the behavior of ferrofluids when subjected to a combination of thermal and hydrodynamic forces, providing practical insights into optimizing ferrofluid applications in cutting-edge industrial processes, energy systems, and advanced thermal technologies.

1. Introduction

Due to their magnetic properties, ferrofluids have become one of the most important research areas as they have many applications in the fields of engineering, medicine and advanced technologies [1]. The fluids are composed of nanoscale ferrite particles in a liquid carrier that make them behave in a different way in the presence of magnetic fields [2]. The use of nanoparticles like ferrite with motile microorganisms increases the efficiency of heat transfer and the flow rate in the ferrofluid systems [3]. This synergy enhances the drag and the heat-transfer characteristics in creeping flow regimes, where the viscous forces dominate the flow [4]. On the other hand, in a regime where the advective forces are greater than the viscous forces, the drag decreases and so does the heat transfer. The duality of behavior is the basis for many modern studies [5].

Previous studies by researchers such as Neuringer and Sivakumar have examined the magnetic and thermal gradients of ferrofluid flows, and found that they can be used in a variety of targeted applications including cooling, catalysis, and biomedical systems [6]. The result of these studies has paved the way to the understanding of the effects of external factors such as magnetic field and radiative heat transfer on ferrofluid dynamics [7]. The insights gained are crucial for the optimization of thermal systems for many industrial and medical applications, such as targeted drug delivery and hyperthermia therapy [8].

A significant amount of research has been conducted on chemical reactions in boundary-layer flows, as they are important in industrial and environmental applications [9]. Homogeneous (bulk) and heterogeneous (surface) reactions also are important in catalytic processes, biomedical fluid dynamics, and hydrometallurgy [4]. Modelling studies, such as those conducted by Chaudhary and Kameswaran, have looked at the impacts of these reactions under different scenarios, and have revealed just how significant these reactions can be for species concentration and fluid flow. For example, more intense homogeneous reactions near surfaces decrease the concentration of reactive species, while more intense heterogeneous reactions increase mass transfer efficiencies [11]. These studies have applications to the optimization of cooling towers, chemical reactors, and systems in environmental engineering [12].

Ferrofluids, first introduced by Stephen in 1965, have undergone many changes since that time in their application. Ferrofluids have been used in medical and safety applications, as early as works by Odenbach and Shliomis, demonstrating the ability to control the viscosity of ferrofluids under magnetic field [13]. This knowledge has been developed further in recent research, including that of Nadeem and Hussanan [14], which examines their rotational properties, convective heat transfer coefficients and thermal stability. This discovery has facilitated the use of ferrofluids in magnetic cooling systems, biomedical applications and advanced manufacturing [15]. Another area of interest has been the study of radiative heat transfer, particularly in the context of space technology, aerodynamics, and environmental engineering [16]. Khan and Mabood [17] have modeled flow of radiative nanofluid and proved that these nanofluid flows exhibit high thermal efficiencies under different surface conditions. Modeling heat sources or sinks further generates our understanding of the behavior of fluid, and can be used in a variety of applications such as textiles, atmospheric sciences, and chemical engineering, etc. [18].

In recent years, the use of machine learning (ML) has transformed the research on fluid dynamics and thermal analysis. With its capabilities for dealing with massive amounts of data and identifying complex patterns, ML has proven to be an invaluable tool in the prediction of thermal characteristics and flow behaviors [19]. In their work, Chen and Zhang showed that the thermal conductivity of nanofluids can be predicted with unprecedented accuracy using a ML model [20]. Gupta and Garg also used ML techniques to improve heat transfer predictions, demonstrating the potential of data-driven approaches to optimize nanofluid systems in a similar manner [20]. Raissi and Karniadakis

presented Physics-Informed Neural Networks (PINNs), which has also moved the bridge between theoretical modelling and data-driven insights [21]. These networks can solve the partial differential equations, making a robust prediction in complex fluid flow systems [22]. Wang and Zhang further endorsed the idea by incorporating data driven modelling in fluid mechanics for the development of advanced predictive analytics in thermal systems [23]. ML also has applications beyond predictive modeling in the realm of heat transfer and fluid flow. It has been pointed out by researchers such as Sadeghi and Mohammadi how it can be used in order to optimize an engineering system [17, 25] and by Yoon and Lee how it can be used to design a nanofluid with enhanced thermal properties [24]. As stated by Li and Zhang, deep learning techniques hold great potential to tackle heat transfer problems, providing a complete framework for future explorations [25].

Despite the progress made, there are still many challenges that must be overcome to fully realize the potential of ferrofluids [26]. There is a need for comprehensive models which incorporate experimentation with computational understanding of thermal, chemical and magnetic properties [27]. Some applications, such as ferrofluid cooling systems, magnetic drug delivery systems, and energy conversion systems, require precision and efficiency, making this need particularly important [28]. The application of machine learning in ferrofluid research is a paradigm shift that will allow predictive and explanatory models to be designed [29]. The use of experimental data and advanced computational methods such as neural networks and the Random Forest algorithm allows researchers to decipher the intricate relationships driving the behavior of ferrofluids [30]. This will not only contribute to the scientific progress of the human kind but will also provide solutions for their use in real life.

2. Research Motivation and Significance

a) In the study, a powerful numerical method, called the New Iterative Method (NIM), is used to solve complex partial differential equations that represent the ferrofluid and nanofluid systems [31]. The method is used to solve the difficulty of non-linear behavior in the fluid flow and has been proven to obtain a reliable and stable prediction of the velocity, temperature and concentration variation when subjected to various conditions [32].

b) To harness the complex interactions among the important parameters such as the thermal Rayleigh number, the ferrohydrodynamic interactions, and the concentration of nanoparticles, this research combines the capabilities of neural networks and random forests—a powerful class of machine learning algorithms. This allows the accurate prediction and complete understanding of the dynamics of this nanofluid [34].

c) The research work involves study of the interplay of thermal, magnetic and hydrodynamic factors in ferrofluid system. These insights are crucial to improve performance of industrial and biomedical systems such as cooling systems, drug delivery systems, and power management systems [35].

d) Combining NIM's numerical precision with machine learning's predictive capabilities offers a novel hybrid framework. This dual approach improves the understanding and control of the complex behavior of such nanofluid, pushing the limits of current research [36].

The results are essential for the development of efficient thermal management systems, for the optimization of technologies with ferrofluids and for the development of thermal processes in a wide variety of applications, including medicine, energy conversion and aerospace.

3. Mathematical Problem Descriptions

A two-dimensional, incompressible, and electrically non-conducting ferrofluid flows over an impermeable, linearly stretching sheet $u_w(x)$. Stretching is induced by applying pressure to the sheet $\hat{y} = 0$, proportional to the distance from the origin. [37] A magnetic dipole is positioned at a distance b along the y-axis from the x-axis, creating a magnetic field that saturates the ferrofluid in the positive x-direction [38].

The Curie temperature (T_c) is assumed to be higher than the stretching sheet's temperature (T_w), while the ambient fluid temperature matches the temperature away from the sheet. Beyond (T_c), the ferrofluid loses its magnetic properties. Conversely, the temperature $T = T_\infty$ is thought to equal the fluid element's temperature away from the sheet. where $T_\infty > T_c > T_w$ .The fluid over Tc is not magnetically able. $\hat{T}_w = \hat{T}_o + \hat{b}_1 x,\ \hat{T}_\infty = \hat{T}_o + \hat{b}_2 x$

[39].The effects of heat generation or absorption are considered negligible. The governing boundary layer equations are formulated to describe the ferrofluid's flow and heat transfer dynamics, integrating the influence of magnetic dipole-induced fields, temperature gradients, and surface stretching. These equations provide a mathematical framework to analyze the velocity, temperature, and heat transfer behavior in this ferrofluid system.

$$\frac{\partial \hat{u}}{\partial \hat{x}} + \frac{\partial \hat{v}}{\partial \hat{y}} = 0 \tag{1}$$

$$\hat{u}\frac{\partial \hat{u}}{\partial \hat{x}} + \hat{v}\frac{\partial \hat{u}}{\partial \hat{y}} - \frac{\mu_0 M}{\rho}\frac{\partial H}{\partial \hat{x}} = -\frac{1}{\rho_f}\frac{\partial \hat{p}}{\partial \hat{x}} + \hat{v}\frac{\partial^2 \hat{u}}{\partial y^2} + \frac{1}{\rho_f}(1 - C_\infty)\rho_f \beta g(T - T_\infty) - (\rho_p - \rho_f)g(C - C_\infty) - (n - n_\infty)g\Delta\rho \tag{2}$$

$$\hat{u}\frac{\partial \hat{T}}{\partial \hat{x}} + \hat{v}\frac{\partial \hat{T}}{\partial \hat{y}} + \frac{\mu_0 \hat{T}}{\hat{\rho}}\left(\hat{u}\frac{\partial \hat{H}}{\partial \hat{x}} + \hat{v}\frac{\partial \hat{H}}{\partial \hat{y}}\right)\frac{\partial \hat{M}}{\partial \hat{T}} = \alpha\frac{\partial^2 \hat{T}}{\partial \hat{y}^2} + \tau\left(D_B\frac{\partial C}{\partial \hat{y}}\frac{\partial \hat{T}}{\partial \hat{y}} + \frac{D_T}{\hat{T}_\infty}\frac{\partial \hat{T}}{\partial \hat{y}}\frac{\partial \hat{T}}{\partial \hat{y}}\right) \tag{3}$$

$$\hat{u}\frac{\partial C}{\partial \hat{x}} + \hat{v}\frac{\partial C}{\partial \hat{y}} = D_B\frac{\partial^2 C}{\partial \hat{y}^2} + \frac{D_T}{\hat{T}_\infty}\frac{\partial^2 \hat{T}}{\partial \hat{y}^2} \tag{4}$$

$$\hat{u}\frac{\partial \hat{a}}{\partial \hat{x}} + \hat{v}\frac{\partial \hat{a}}{\partial \hat{y}} = D_A\left(\frac{\partial^2 \hat{a}}{\partial \hat{x}^2} + \frac{\partial^2 \hat{a}}{\partial \hat{y}^2}\right) + \frac{D_T}{\hat{T}_\infty}\left(\frac{\partial^2 \hat{T}}{\partial \hat{x}^2} + \frac{\partial^2 \hat{T}}{\partial \hat{y}^2}\right) - k_c ab^2 \tag{5}$$

$$\hat{u}\frac{\partial \hat{b}}{\partial \hat{x}} + \hat{v}\frac{\partial \hat{b}}{\partial \hat{y}} = D_B\left(\frac{\partial^2 \hat{b}}{\partial \hat{x}^2} + \frac{\partial^2 \hat{b}}{\partial \hat{y}^2}\right) + \frac{D_T}{\hat{T}_\infty}\left(\frac{\partial^2 \hat{T}}{\partial \hat{x}^2} + \frac{\partial^2 \hat{T}}{\partial \hat{y}^2}\right) - k_c ab^2 \tag{6}$$

For a boundary value problem, it is assumed that the following boundary conditions are admissible

$$\begin{cases} \hat{U}_{y=0} = \hat{U}_w(\hat{x}) = \hat{a}x \\ \hat{U}_{y\to\infty} \to \hat{U}_e(\hat{x}) = 0 \\ \hat{v}_{y=0} = 0 \\ \hat{T}_{y=0} = \hat{T}_w \\ C|_{y=0} = C_w \\ n|_{y=0} = n_w \\ \hat{T}_{y\to\infty} \to T_\infty = \hat{T}_c \\ C|_{y\to\infty} \to C_\infty \\ n|_{y\to\infty} \to n_\infty \end{cases} \tag{7}$$

In equation (7) $U_w x$ describes stretching velocity whereas T_∞ determines the fluid's ambient temperature.

The presence of a magnetic dipole generates a magnetic field that influences the flow behavior of ferrofluids. This effect is characterized by a magnetic scalar potential, mathematically expressed to capture the impact of the dipole on the ferrofluid dynamics [40].

$$\hat{\chi} = \frac{\hat{\gamma}}{2\pi}\frac{\hat{x}}{\hat{x}^2 + (\hat{y} + \hat{b})^2} \tag{8}$$

The magnetic field's components include

$$\hat{H}_x = -\frac{\partial \hat{\chi}}{\partial \hat{x}} = \frac{\hat{\gamma}}{2\pi}\frac{\hat{x}2 - (\hat{y} + \hat{b})^2}{\left(\hat{x}^2 + (\hat{y} + \hat{b})^2\right)^2} \tag{9}$$

$$\hat{H}_y = -\frac{\partial \hat{\chi}}{\partial \hat{y}} = \frac{\hat{\gamma}}{2\pi}\frac{2\hat{x}(\hat{y} + \hat{b})}{\left(\hat{x}^2 + (\hat{y} + \hat{b})^2\right)^2} \tag{10}$$

$$\hat{H} = \sqrt{\left(\frac{\partial \hat{\chi}}{\partial \hat{x}}\right)^2 + \left(\frac{\partial \hat{\chi}}{\partial \hat{y}}\right)^2} \quad (11)$$

Putting the value of equations (9) and (10) in eq (11), terms up to order x^2 and expanding in powers of x. we arrive to the following equations, after retaining

$$\frac{\partial \hat{H}}{\partial \hat{x}} = -\frac{\hat{\gamma}}{2\pi}\frac{2\hat{x}}{(\hat{y}+\hat{b})^4} \quad (12)$$

$$\frac{\partial \hat{H}}{\partial \hat{y}} = \frac{\hat{\gamma}}{2\pi}\left(-\frac{4\hat{x}^2}{(\hat{y}+\hat{b})^5} + \frac{2}{(\hat{y}+\hat{b})^3}\right) \quad (13)$$

The linear expression below estimates the influence of magnetization M with temperature T.

$$\hat{M} = \hat{K}\left(\hat{T} - \hat{T}_\infty\right) \quad (14)$$

The variables without dimensions are now introduced.

$$\hat{\Psi}(\xi) = \left(\frac{\hat{a}\hat{\mu}}{\hat{\rho}}\right)^{\frac{1}{2}}\hat{x}f(\xi), \xi = \hat{y}\left(\frac{\hat{\rho}\hat{a}}{\hat{\mu}}\right)^{\frac{1}{2}} \quad (15)$$

$$\hat{\theta}(\xi) = \frac{\hat{T}-\hat{T}_c}{\hat{T}_w-\hat{T}_c}, \phi(\xi) = \frac{\hat{C}-\hat{C}_\infty}{\hat{C}_w-\hat{C}_\infty}, j(\xi) = \frac{\hat{n}-\hat{n}_\infty}{\hat{n}_w-\hat{n}_\infty} \quad (16)$$

Here $\hat{\theta}_1\left(\hat{\eta}, \hat{\xi}\right)$ *and* $\hat{\theta}_2\left(\hat{\eta}, \hat{\xi}\right)$ demonstrate a temperature without dimensions, and the equivalent dimensionless coordinates are. The stream function and the corresponding velocity components u and v are formulated to inherently satisfy the continuity equation [41].

$$\hat{u} = \frac{\partial \psi}{\partial \hat{y}} = u_w f'(\xi), \quad (17)$$

$$\hat{v} = -\frac{\partial \psi}{\partial \hat{x}} = -\sqrt{\frac{\mu \hat{a}}{\hat{\rho}}}f(\xi) \quad (18)$$

Where as

$$f''' - f'^2 + ff'' - \frac{2\hat{\beta}_f\hat{\theta}_1}{(\xi+\gamma)^4} + \hat{\lambda}_b\theta - \hat{R}_n\phi - \frac{\hat{R}_b}{\hat{L}_b}\hat{j} - \hat{R}_m = 0 \quad (19)$$

$$\hat{\theta}_1'' + \hat{\mathrm{P}}\mathrm{rf}\,\hat{\theta}_1' + \frac{2\lambda\hat{\beta}f\left(\hat{\theta}_1 - \hat{\varepsilon}\right)}{\left(\xi+\gamma\right)^3} + \hat{N}_b\hat{\theta}'\hat{\phi}' + \hat{N}_t\hat{\theta}'^2 = 0 \quad (20)$$

$$\hat{\phi}'' + \hat{\mathrm{S}}\hat{\mathrm{c}}\hat{\mathrm{f}}\,\hat{\phi}' + \frac{\hat{N}_t}{\hat{N}_b}\hat{\theta}'' = 0, \quad (21)$$

$$\hat{j}'' + \hat{L}_b\hat{f}\,\hat{j}' - P_e\left(\hat{\phi}''\hat{j} + \hat{\phi}'\hat{j}'\right) = 0 \quad (22)$$

$$\hat{f}\left(\xi\right) = 0, \hat{f}'\left(\xi\right) = 1, \hat{\theta}_1\left(\xi\right) = 1, \hat{\phi}\left(\xi\right) = 1, \hat{j}\left(\xi\right) = 1 at\ \xi = 0 \quad (23)$$

$$\hat{f}'\left(\xi\right) \to 0, \hat{\theta}\left(\xi\right) \to 0, \hat{\phi}\left(\xi\right) \to 0, \hat{j}\left(\xi\right) \to 0\ \ when\ \xi \to \infty \quad (24)$$

In the given system of nonlinear equations Table 1, the parameters are defined as follows: "β" Ferrohydrodynamic interaction parameter, "Pr" Prandtl number, "S" Thermal stratification parameter, "R" Ratio parameter, "λ" Viscous dissipation parameter, Curie temperature "Tc"[42]

Parameters;

$$\lambda_b = \frac{\hat{\rho}_f\hat{\beta}_g(1-C_\infty)(\hat{T}_w-\hat{T}_c)}{\hat{\mu}\hat{\alpha}_f}, R_n = \frac{\hat{g}(\hat{\rho}_p-\hat{\rho}_f)(C_w-C_\infty)}{\hat{\mu}\hat{\alpha}_f}, R_b = \frac{\hat{g}\Delta\hat{\rho}}{\hat{\mu}D_m} \quad (25)$$

$$\hat{N}_b = \frac{\hat{\tau}\hat{D}_B(C_w-C_\infty)}{\hat{\alpha}_f}, \hat{R}_m = \frac{\hat{g}\left(\hat{\rho}_p n_w + \hat{\rho}_f(1-n_w)\right)}{\hat{\mu}\hat{\alpha}_f} \quad (26)$$

$$\hat{\varepsilon} = \frac{\hat{T}_c}{\hat{T}_w-\hat{T}_c}, \hat{S}_c = \frac{\hat{v}_f}{\hat{D}_B}, \hat{P}_r = \frac{\hat{v}_f}{\hat{\alpha}_f}, \hat{N}_t = \frac{\hat{\tau}\hat{D}_T(\hat{T}_w-\hat{T}_c)}{\hat{\alpha}_f\hat{T}_c} \quad (27)$$

$$\widehat{\beta}_f = \frac{\gamma}{2\pi}\frac{\hat{\mu}_0\widehat{K}(\widehat{T}_w-\widehat{T}_c)\hat{\rho}_f}{\hat{\mu}^2_c}, \hat{\lambda} = \frac{\hat{\mu}^2}{\hat{\rho}_f\widehat{K}(\widehat{T}_w-\widehat{T}_c)} \quad (28)$$

$$\hat{\gamma} = \sqrt{\frac{\hat{\alpha}\hat{\rho}_f b^2}{\hat{\mu}}}, \hat{L}_b = \frac{\hat{\alpha}_f}{\hat{v}_f D_m}, \widehat{P}_e = \frac{bW_c}{D_m} \quad (29)$$

$$R = \frac{\widehat{Q}}{S}, Pr = \frac{\hat{v}}{\alpha}, \varepsilon = \frac{\widehat{T}_\infty}{\widehat{T}_0-\widehat{T}_w} \quad (30)$$

$$\widehat{\beta} = \frac{\gamma}{2\pi}\frac{\hat{\mu}_0\widehat{K}(\widehat{T}_0-\widehat{T})}{\hat{\mu}^2}, \hat{S}_1 = \frac{\hat{b}_2}{\hat{b}_1} \quad (31)$$

$$\hat{\lambda} = \frac{S\hat{\mu}^2}{\hat{\rho}k(\widehat{T}_0-\widehat{T}_w)}, \hat{\gamma}_1 = \sqrt{\frac{\hat{S}\hat{\rho}\hat{b}^2}{\hat{\mu}}} \quad (32)$$

Nusselt number

$$\widehat{C}_f = \frac{2\hat{\tau}_w}{\hat{\rho}\widehat{U}_w{}^2}, \hat{S}\hat{h}_x = \frac{\hat{x}\gamma_w}{D_B(C_w-C_\infty)}, \widehat{N}u_x = \frac{\hat{x}q_w}{\widehat{k}\ (\widehat{T}_0-\widehat{T}_w)}$$

$$\hat{\tau}_w = \hat{\mu}\frac{\partial\hat{u}}{\partial\hat{y}}\Big|_{y=0}, \hat{q}_w = -\hat{k}\frac{\partial\widehat{T}}{\partial\hat{y}}\Big|_{y=0}, \hat{\gamma}_w = -D_B\frac{\partial\widehat{C}}{\partial\hat{y}}\Big|_{y=0}, \hat{j}_w = -D_m\frac{\partial\hat{n}}{\partial\hat{y}}\Big|_{y=0}$$

Finally, we accomplished the following nondimensional equations

$$\frac{1}{2}\widehat{R}e^{\frac{1}{2}}\widehat{C}_f = f''(0), \widehat{R}e^{\frac{1}{2}}\widehat{N}u_x = -\theta'(0), \widehat{R}e^{\frac{1}{2}}\hat{S}h_x = -\phi'(0), \widehat{R}e^{\frac{1}{2}}\widehat{N}n_x = -j'(0) \quad (33)$$

4. Research Methodology

4.1 New Iterative Method for Nonlinear Equations

In this section, the New Iterative Method (NIM) [43] is emphasized for solving differential equations. Consider the general form of the differential equation:

$$\hat{M}(\hat{x}) = \hat{L}\left(\hat{M}(\hat{x})\right) + \hat{f}(\hat{x}) + \hat{N}\left(\hat{M}(\hat{x})\right) \quad (34)$$

"Where the linear operator is denoted by $\hat{L}, \hat{f}(\hat{x})$ is known function, $\widehat{M}(\hat{x})$ is the unknown function, $\widehat{N}\left(\widehat{M}(\hat{x})\right)$ is the nonlinear operator. Suppose that the solution of the New Iterative method of Eq. (23) is of the form ".

$$\hat{M}(\hat{x}) = \sum_{i=0}^{\infty}\hat{M}_i \quad (35)$$

As $\hat{L}$ is a linear operator, therefore

$$\hat{L}\left(\sum_{i=0}^{\infty}\hat{M}_i\right) = \sum_{i=0}^{\infty}\hat{L}\left(\hat{M}_i\right). \quad (36)$$

The non-linear operator is given by[47]

$$\hat{N}\left(\sum_{i=0}^{\infty}\hat{M}_i\right) = \hat{N}\left(\hat{M}_0\right) + \sum_{i=1}^{\infty}\{\hat{N}\left(\sum_{j=0}^{i}\hat{M}_j\right) - \hat{N}\left(\sum_{j=0}^{i-1}\hat{M}\right)\} = \sum_{i=0}^{\infty}E_i. \quad (37)$$

Where $E_0 = \widehat{N}(\widehat{W}_0)$ and

$$E_i = \left\{\hat{N}\left(\sum_{j=0}^{i}\hat{M}_j\right) - \hat{N}\left(\sum_{j=0}^{i-1}\hat{M}_j\right)\right\} \quad (38)$$

Substituting Eqs (24), (25) and (26) in Eq (19) we obtained

$$\sum_{i=0}^{\infty}\hat{M}_i = \hat{f}(\hat{x}) + \sum_{j=0}^{i}\hat{L}\left(\hat{M}_j\right) + \sum_{i=0}^{\infty}E_i \quad (39)$$

4.2 Integrated Methodology for Hybrid Nanofluid Flow Analysis

This research adopts an innovative methodology that integrates physical modeling and advanced machine

learning techniques to analyze hybrid nanofluid flow influenced by various parameters. The study begins by precisely defining the physical problem, focusing on hybrid nanofluid behavior under key factors such as velocity, temperature, and concentration. Specific boundary conditions are used together with the governing equations (such as those of mass conservation, momentum and energy) to represent the flow domain accurately and the physical properties of the system [44].

In addition to the theoretical framework, data is gathered from numerical simulations or experiments, and used for training and validating the machine learning models. The predictive tool is a Physics-Informed Neural Network (PINN), shown in Fig. 1, which can directly embed physical laws into its learning process. These equations are already included in the network's loss function, so that it complies with basic principles in training with real-world or simulated data. The PINN architecture is optimized to be complex and stable to allow capturing complex relationships within the hybrid nanofluid system.

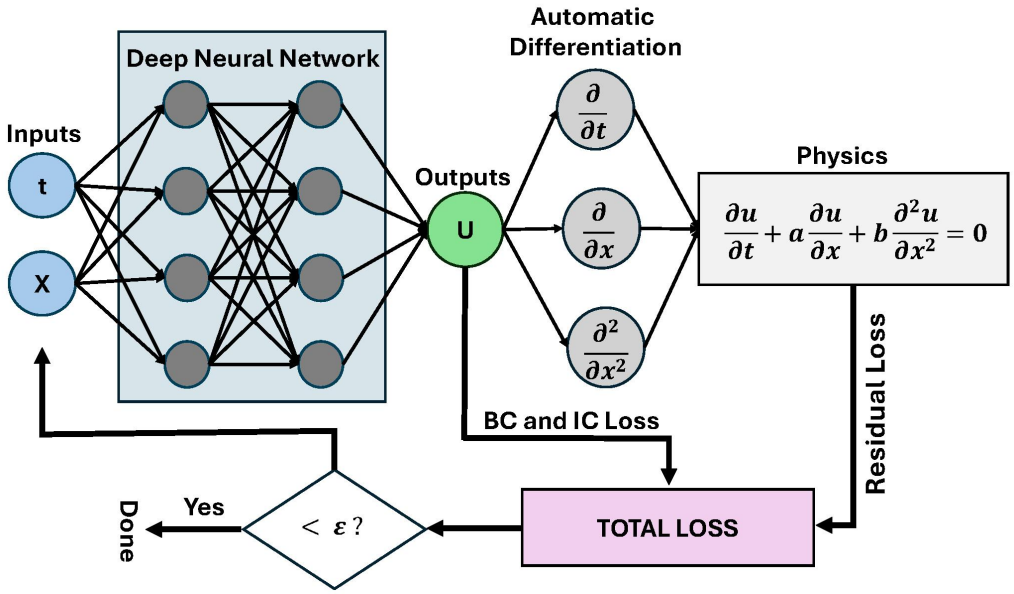

Fig. 1. Physics-Informed Neural Network (PINN)

Concurrently, a Random Forest model [46] is built as a benchmark for comparison. It is a traditional machine learning method specially fine-tuned to forecast flow parameters such as velocity and temperature. The performance of both models is assessed on a structured data set that is split into training and testing sets. This two-model approach guarantees the robustness and accuracy while also offering an understanding of the interaction between physical models and machine learning methods. The research combines data-driven and physics-based approaches to provide a comprehensive understanding of hybrid nanofluid flow, which can be used for future design and optimization [47].

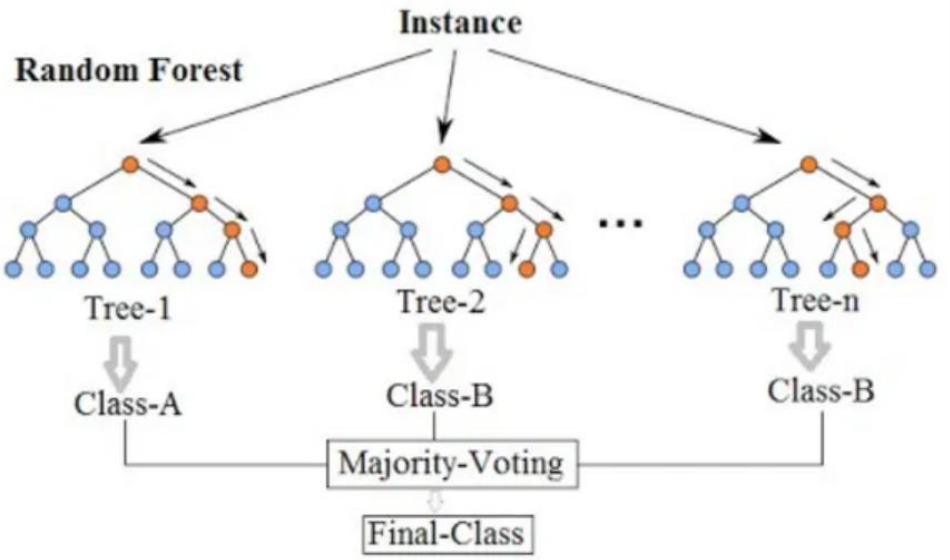

Fig. 2. Structure of Random Forest model

5. Results and Discussion

5.1 *New Iterative Method formulation*

The behavior of the ferrofluids flow over a rotating disc is studied under the influence of various physical parameters, which are analyzed in this section. The effects of important dimensionless parameters associated with ferrohydrodynamic interactions, viscous dissipation, thermal stratification, ratio of basic-density to thermal-density Rayleigh numbers, and distance from the origin to the center of the magnetic dipole have been carefully investigated. Other parameters were held constant during the analysis. The results are shown in:

(a) **Figure 3** show how different factors influence the velocity profile of the ferrofluid. The thermal Rayleigh number increases when the convective heat transfer increases and the velocity profile becomes more clearly defined because of the increased thermal buoyancy. The velocity distribution of the magnetic field is refined due to the Ferrohydrodynamic interactions. Moreover, higher basic density Rayleigh numbers enhance the velocity since there is a buoyancy driven flow. The addition of nanoparticles increases the velocity profile and heat transfer as a result of the greater thermal conductivity of the fluid

(b) The temperature profile dynamics is presented in **Figure 4**, showing the effect of different parameters. Particles tend to migrate along the temperature gradient and the thermophoretic effect is the driving force, leading to increased fluid temperature. In addition, this effect is made more pronounced by the Brownian motion, which provides better mixing and heat transfer. The greater the thermal Rayleigh number, the greater the temperature as it helps to transfer the heat more efficiently. Ferrohydrodynamic interactions also have a positive effect on the temperature distribution, through the improvement of thermal uniformity in the fluid.

(c) In **Figure 5**, the concentration distribution of nanoparticles is studied. The Schmidt number is an indicator of the diffusion rate of nanoparticles and it is observed that lower Schmidt number adversely affects the concentration profile. Thermophoresis, however, tends to concentrate the nanoparticles in the higher temperature regions, leading to concentration enhancements in the local area. This is further aided by the Brownian motion which helps to mix the fluid more thoroughly and spreads the nanoparticles more evenly.

(d) **Figure 6** shows the effect of chemical reactions on the system, with emphasis in the autocatalytic process. A heterogeneous reaction results in a non-uniform change of reactant concentration, while a homogeneous reaction results in a more uniform change of concentration of reactant(s) throughout the fluid. It is clear that the Schmidt number has a great influence on the mass transfer rate during such reactions and therefore on the overall concentration profile in both types of reaction.

(e) **Figure 7** shows the effect of ferrohydrodynamic interactions on skin friction profiles. The skin friction coefficient is smaller in stronger interaction, signifying a more efficient flow regime, and even better heat transfer.

(f) In **Figure 8,** the influence of the parameters such as Prandtl number, thermal Rayleigh number, and the Brownian motion on the heat transfer are examined. The higher the Prandtl number, the lower the value of the thermal diffusivity of the fluid, which leads to greater heat holding ability in the fluid. Increasing the thermal Rayleigh number enhances heat transfer and the fluid's ability to transfer heat will be further enhanced by Brownian motion, which also helps to mix the fluid**.** Finally,

(g) **Figures 9(a) and 9(b)** show the effects of Schmidt number and Brownian motion on the diffusion of nanoparticles. The performance of ferrofluid systems in a thermal application is greatly affected by both of these parameters, so optimization of both is important for maximizing the fluid's performance.

This work gives good insights into the complex interdependence of the different physical parameters that affect ferrofluid flow and heat transfer. Thermal,

hydrodynamic and chemical interactions play an important role in the optimization of ferrofluids for use in thermal management or energy conversion systems.

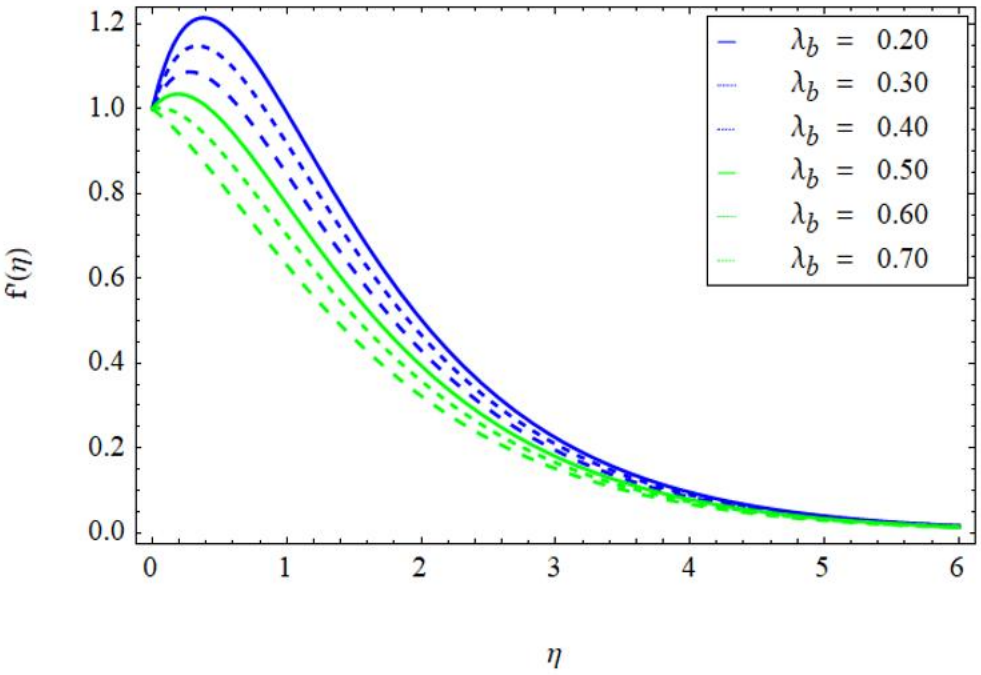

(a)

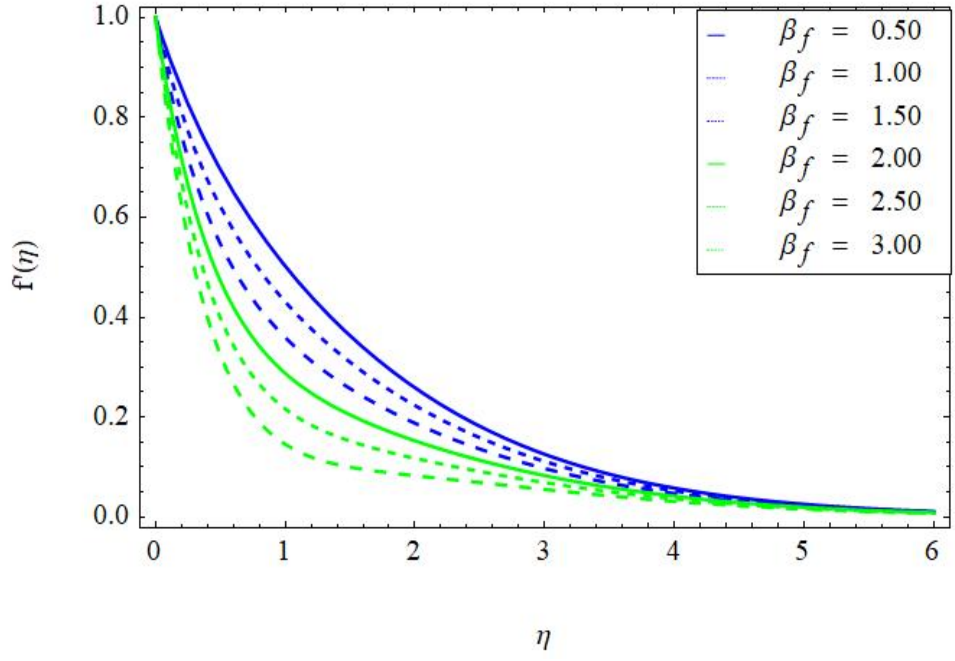

(b)

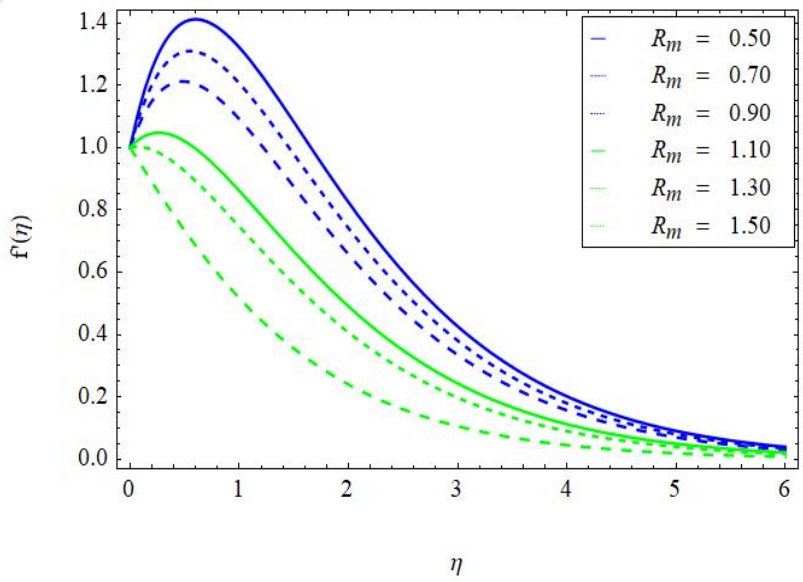

(c)

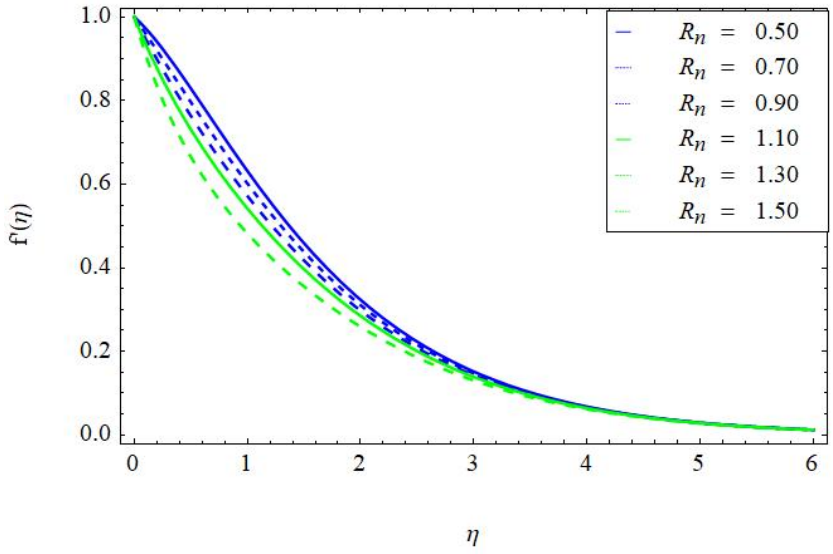

(d)

Figure. 3 Influence of (a) thermal Rayleigh number (b) ferrohydrodynamic interaction (c) basic-density Rayleigh number, and (d) nanoparticle concentration on velocity profile.

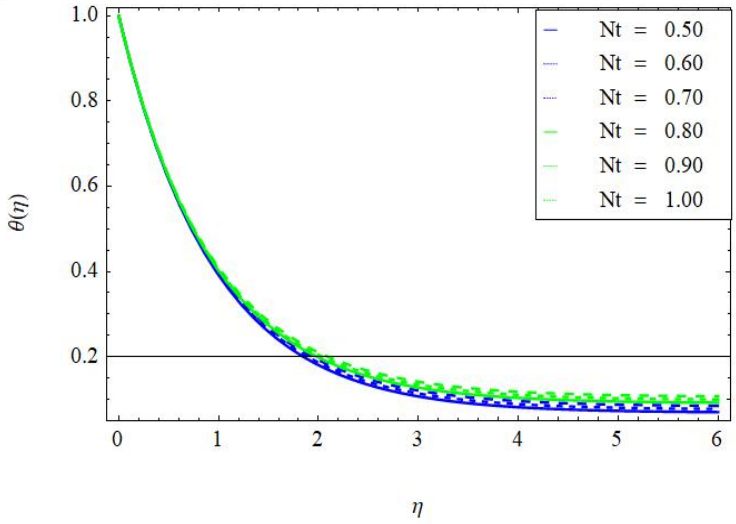
Nt = 0.50
Nt = 0.60
Nt = 0.70
Nt = 0.80
Nt = 0.90
Nt = 1.00
θ(η)
η

(a)

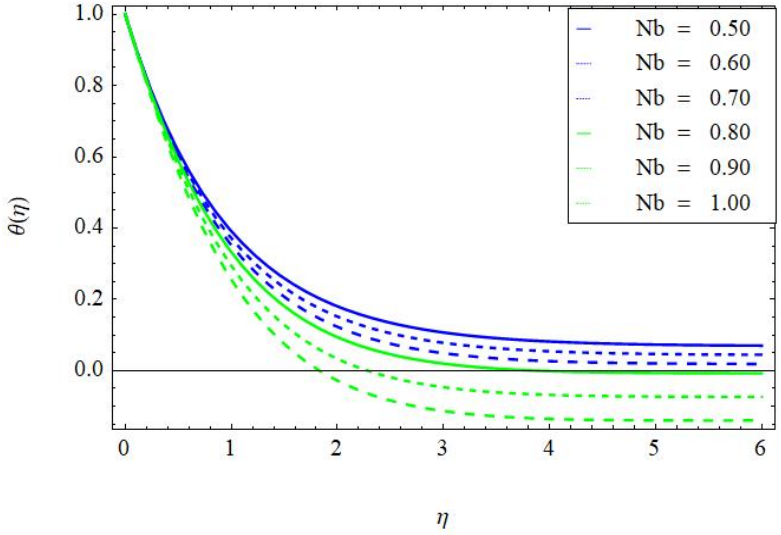
Nb = 0.50
Nb = 0.60
Nb = 0.70
Nb = 0.80
Nb = 0.90
Nb = 1.00
θ(η)
η

(b)

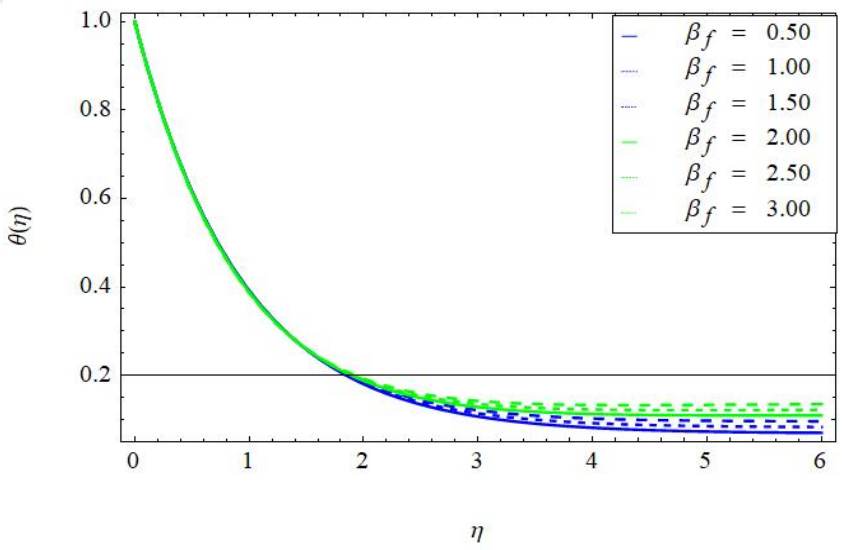

(c)

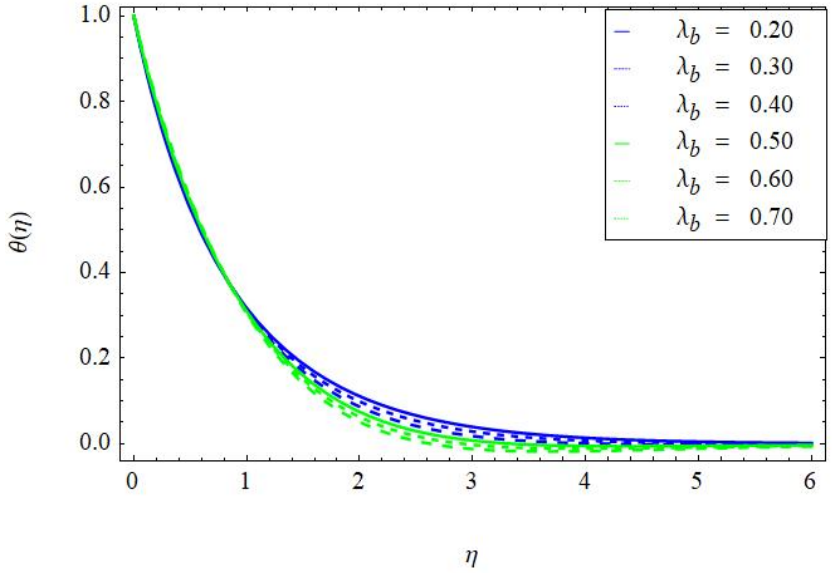

(d)

Figure 4 Influence of (a) thermophoresis (b) Brownian motion (c) ferrohydrodynamic interaction, and (d) thermal Rayleigh number for temperature profile

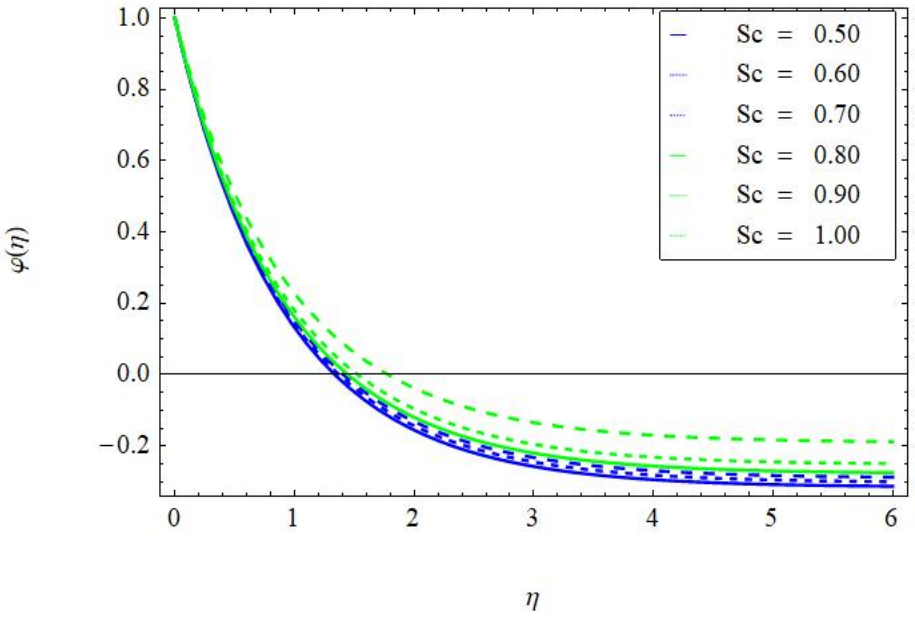
Sc = 0.50
Sc = 0.60
Sc = 0.70
Sc = 0.80
Sc = 0.90
Sc = 1.00
φ(η)
η

(a)

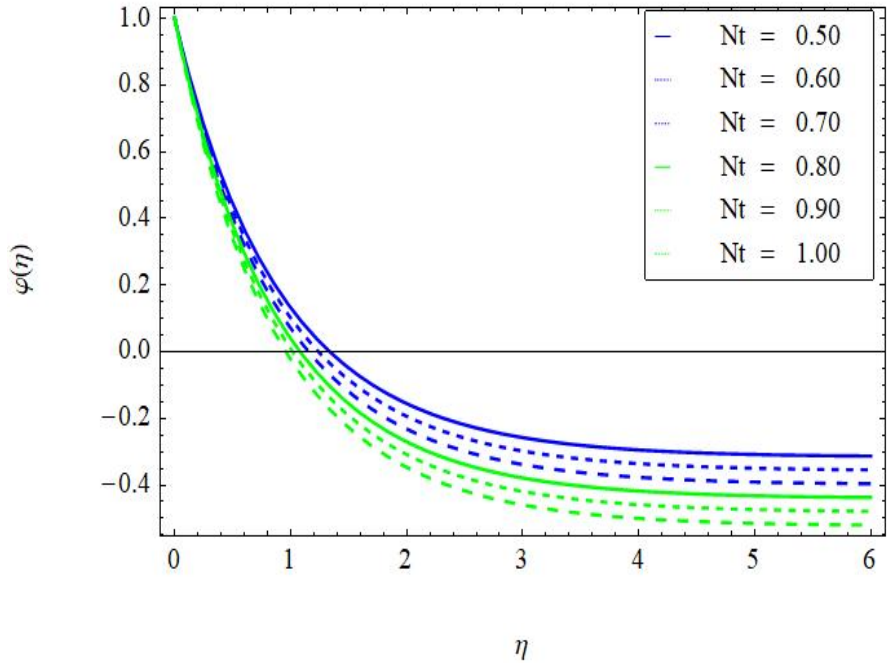
Nt = 0.50
Nt = 0.60
Nt = 0.70
Nt = 0.80
Nt = 0.90
Nt = 1.00
φ(η)
η

(b)

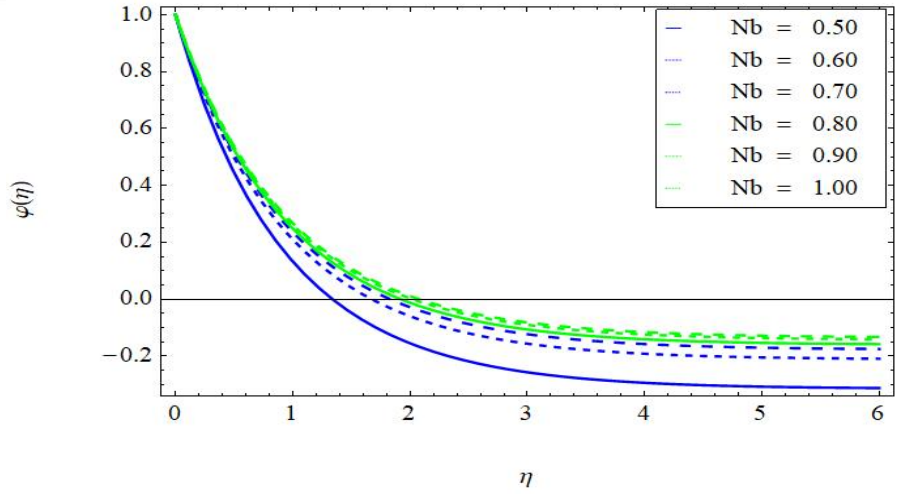

(c)

Figure 5 Influence of (a) Schmidth number (b) thermophoresis, and (c) Brownian motion for the nanoparticle concentration.

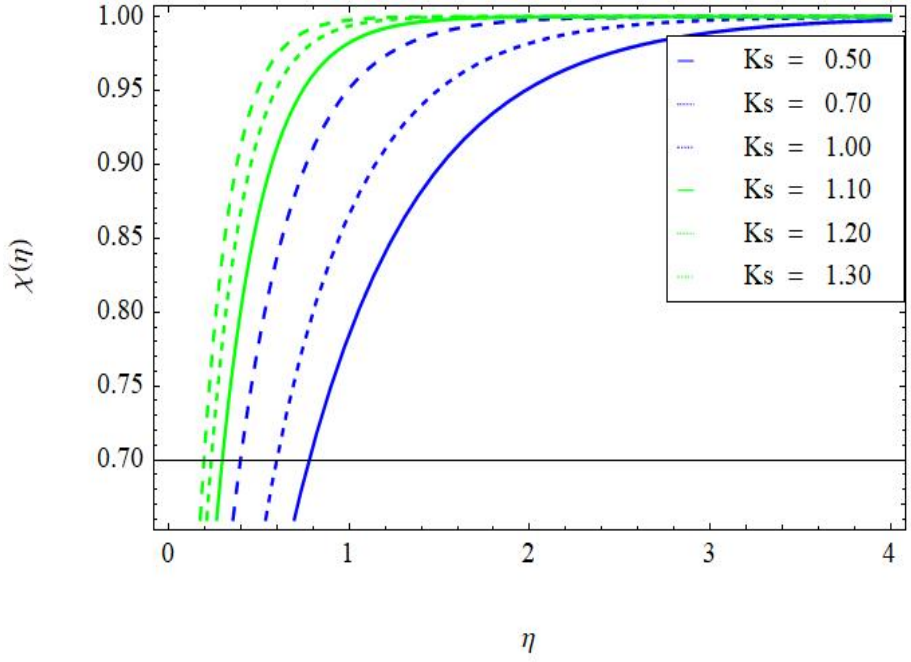

(a)

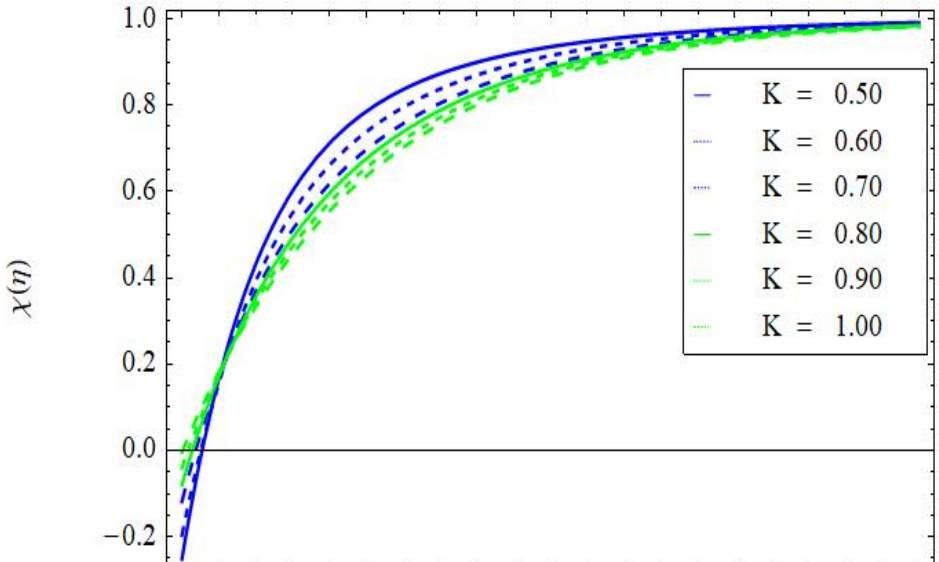

(b)

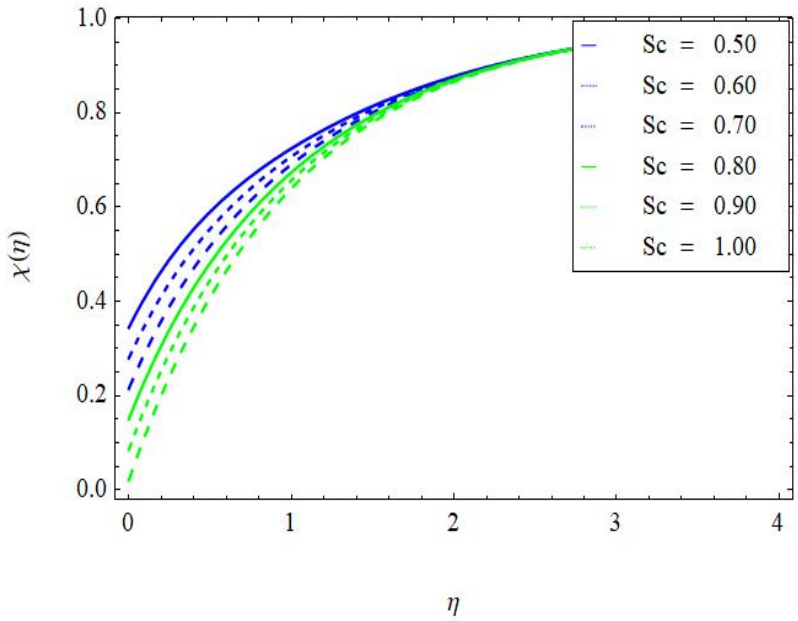

(c)

Figure 5: Influence of (a) heterogeneous chemical reaction (b) homogenous chemical reaction, and (c) Schmidt number for the cubic autocatalysis chemical reaction profile.

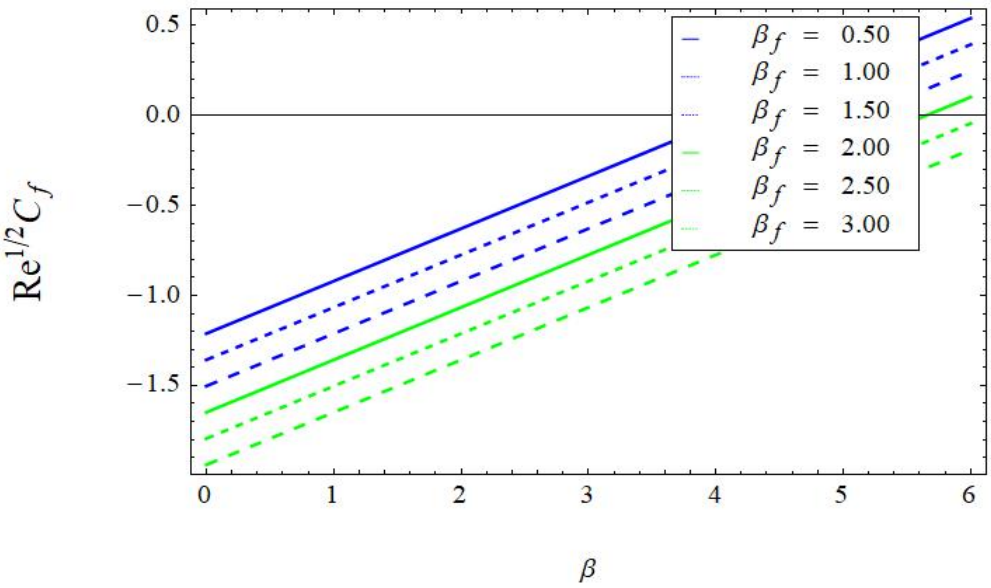

Figure 6: Impact of ferrohydrodynamic interaction for Skin friction profile.

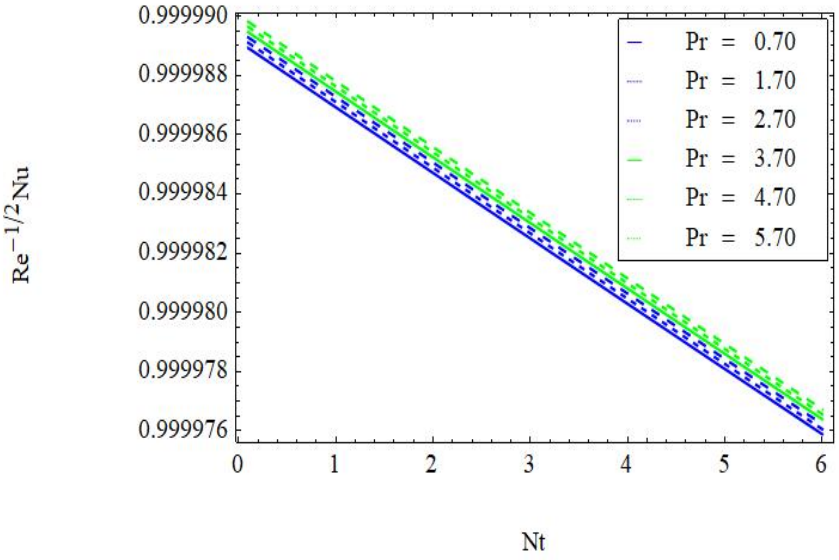

(a)

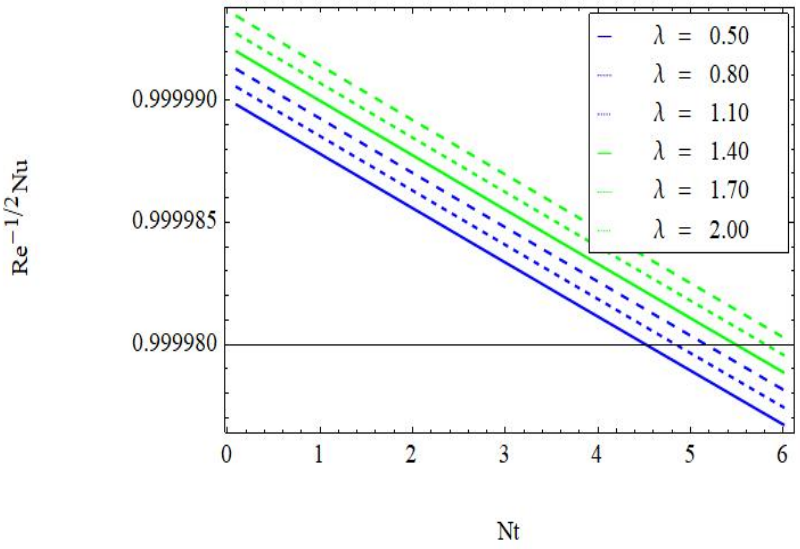

(b)

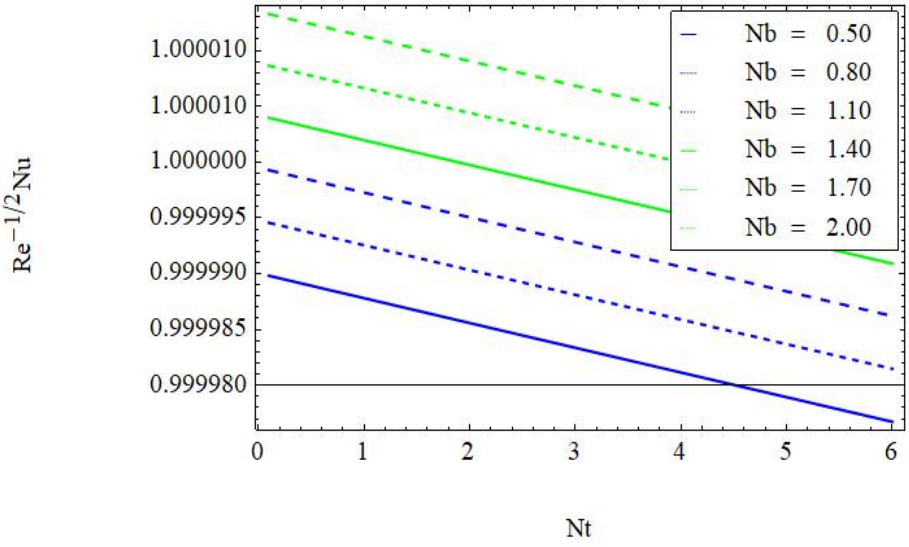

(c)

Figure 7 Influence for (a) Prandtl number (b) thermal Rayleigh number, and (c) Brownian motion.

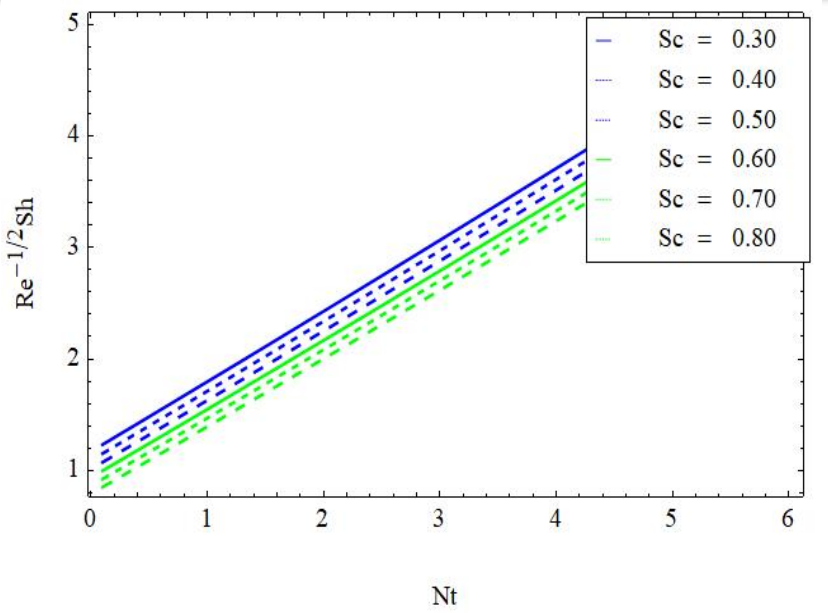

(a)

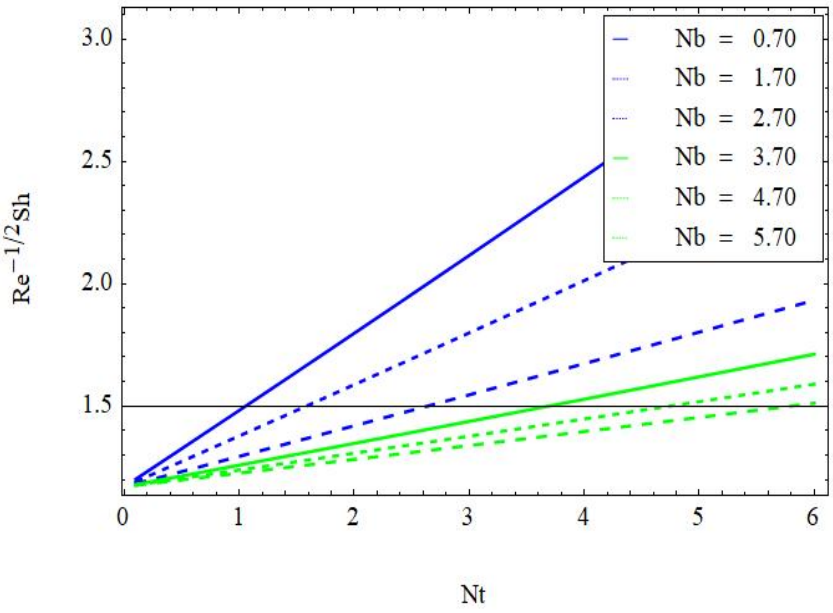

(b)

Figure 8 Influence of (a) Schmidt number, (b) Brownain motion

5.2 Machine Learning model Formulation

This section presents the outcomes of our numerical models, designed to predict the behavior of ferrofluid flow under various conditions. We specifically focused on understanding how parameters such as the thermal Rayleigh number, ferrohydrodynamic interactions, and nanoparticle concentrations influence the velocity and temperature of the ferrofluid. Real data were incorporated into our models so that the accuracy of the predictions could be judged and a better understanding of the interactions between these was achieved. Both models Physics-Informed Neural Network (PINN) and Random Forest demonstrated strong predictive capabilities, accurately forecasting the velocities and temperatures across different scenarios.

The velocity profiles were reproduced in both models despite variations of parameters such as the

thermal Rayleigh number and ferrohydrodynamic interactions. For example, at lower thermal Rayleigh numbers, the velocity predicted was close to the actual velocity with very little error. This high level of accuracy was maintained even with the increase in Rayleigh number and concentration of nanoparticles, thus highlighting the robustness of our models. The same level of accuracy was found for temperature predictions. The discrepancies between the predicted and actual temperature were quite small at both low and high values of thermal Rayleigh numbers. Such consistency in forecast of temperature is essential in the knowledge of heat transfer in ferrofluid, especially in thermal management application.

Understanding Key Parameters

From our analysis, we find that the ferrohydrodynamic interaction and concentrations of nanoparticles influence the flow behavior and thermal properties of the ferrofluid significantly: With a greater ferrohydrodynamic interaction, the fluid velocity is higher, caused by a stronger influence of the magnetic field on the fluid. The effects of the velocity and temperature distributions on the velocity and important effects of the variation of the concentration of nanoparticles was demonstrated, showing that it is of great importance in optimizing the performance of ferrofluids. Both models showed high accuracy, so we performed error analysis to further evaluate the performance of both models. The average errors calculated for the velocity and temperature predictions were found to be low, thus showing that the models are reliable. There is scope for further improvement, however, including the ability to make more precise predictions by adjusting model parameters, and by incorporating other physical factors.

The velocity components, temperature, stream function and concentration were very well predicted at various spatial locations by the PINN model. This is because the governing physical laws (expressed as PDEs) can be directly coupled to the learning process by the unique capability of PINNs. Therefore, the PINN method was shown to be stable and accurate prediction even in complex fluid dynamics problems.

The velocity, temperature, stream function and the concentration of the nanoparticles were also well predicted with the Random Forest model. Its advantage is due to the fact that it can represent complex, non-linear relationships between parameters. This was slightly different in some parts, however, which could be adjusted with even more tuning, particularly at places where there are sharp variations in data. We identified the following advantages and disadvantages in the two models: The PINN was slightly more accurate at predicting the temperature, as it used a physics-based learning approach, while the other model was simpler and more compact. The Random Forest model gave good approximation for velocity and concentration, it showed its potential to work with nonlinearities. In regions with steep gradients, however, the PINN model had more accurate predictions.

The Random Forest model is less complex and therefore is better suited for situations where faster predictions are required. The PINN, on the other hand, is more intensive but is more accurate, particularly in complex fluid dynamics. Overall, our study shows that physical models and machine learning techniques can complement each other to make high-accuracy predictions of ferrofluid behavior. The PINN model and the Random Forest model are both very useful to researchers and engineers using ferrofluids. Both models will be suitable based on the application, with accuracy versus computational efficiency.

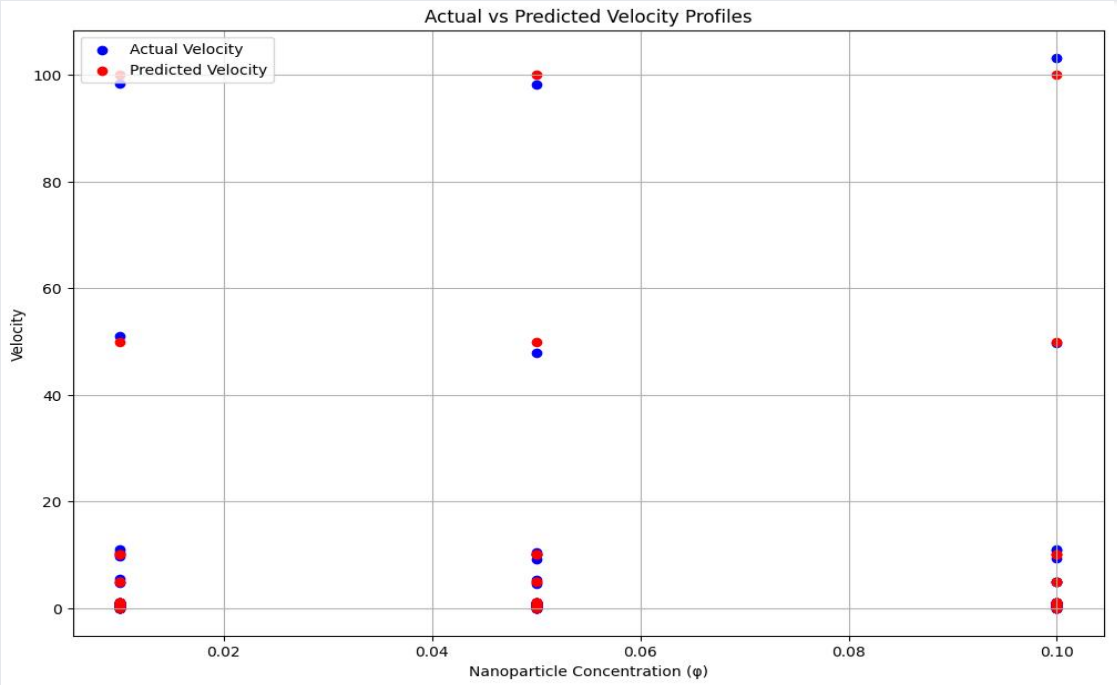

(a)

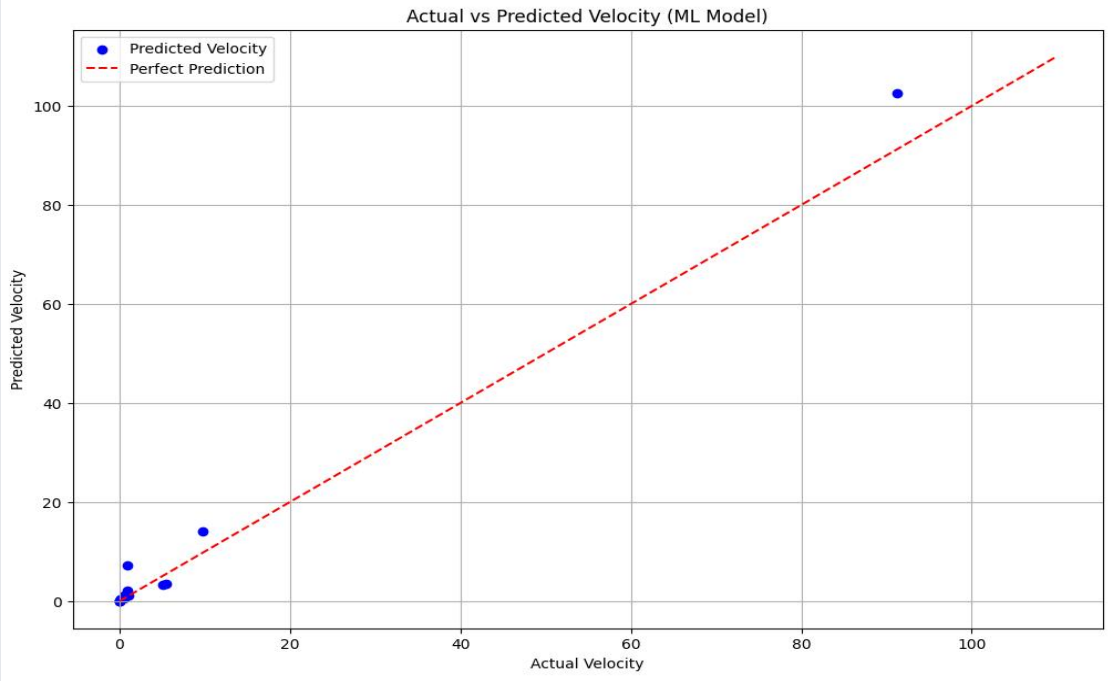

(b)

Figure9; Actual and predicted (a) velocity profile (b) velocity profile (ML).

Table 2: This table shows the values for the ferrofluid flow study with the actual and predicted velocities calculated based on various parameters, such as Rayleigh numbers and nanoparticle concentrations.

Index	Thermal Rayleigh	Ferrohydrodynamic Interaction (β)	Basic-Density	Nanoparticle Concentration (φ)	Actual Velocity	Predicted Velocity

	Number (Ra)		Rayleigh Number (Rm)			
0	1000	0.1	1000	0.01	0.102172	0.099999
1	1000	0.1	1000	0.05	0.098397	0.099995
2	1000	0.1	1000	0.10	0.101251	0.099990
3	1000	0.1	10000	0.01	0.010932	0.010000
4	1000	0.1	10000	0.05	0.010077	0.010000
...	...	...	...	...	...	...
76	100000	1.0	10000	0.05	9.651442	9.999950
77	100000	1.0	10000	0.10	9.801951	9.999900
78	100000	1.0	100000	0.01	1.036378	1.000000
79	100000	1.0	100000	0.05	1.070382	1.000000
80	100000	1.0	100000	0.10	0.962720	0.999990

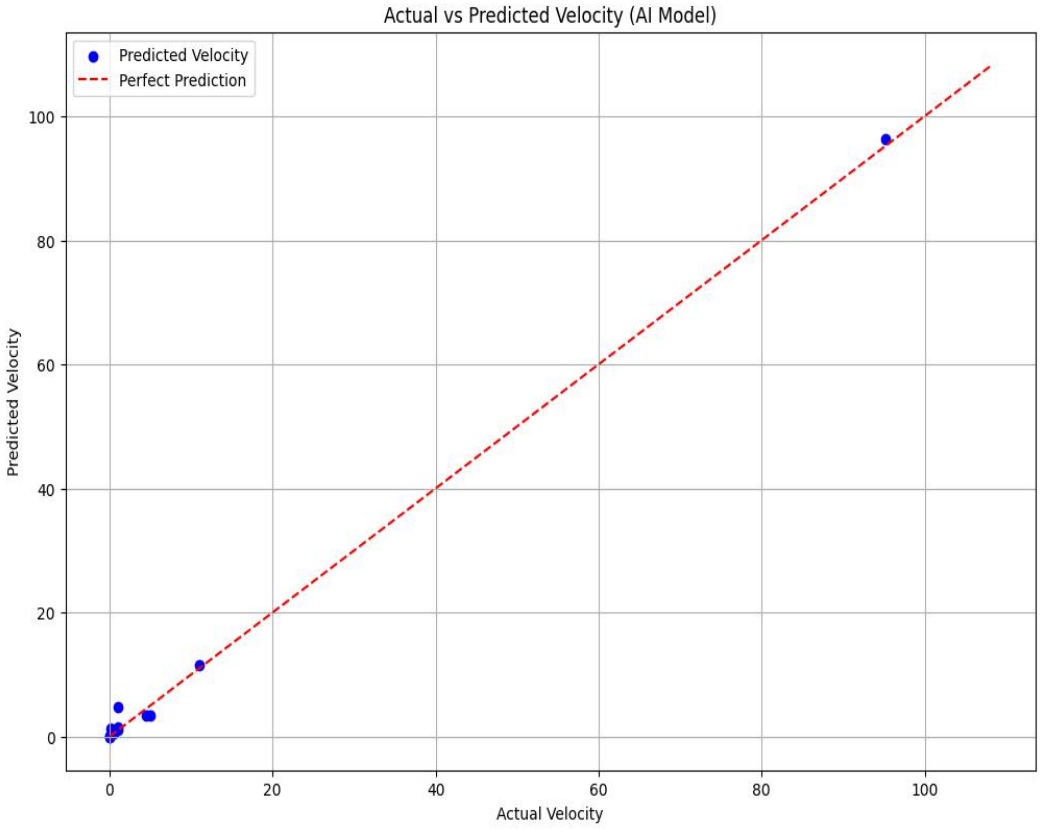

(a)

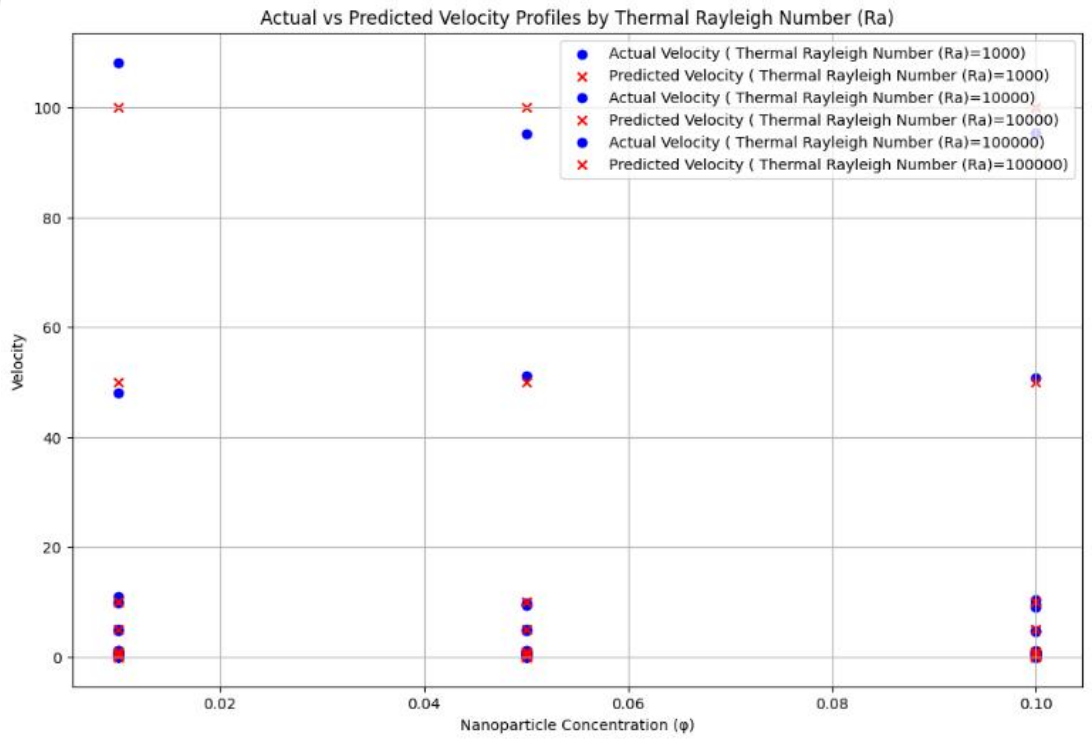
Actual vs Predicted Velocity Profiles by Thermal Rayleigh Number (Ra)
Actual Velocity (Thermal Rayleigh Number (Ra)=1000)
Predicted Velocity (Thermal Rayleigh Number (Ra)=1000)
Actual Velocity (Thermal Rayleigh Number (Ra)=10000)
Predicted Velocity (Thermal Rayleigh Number (Ra)=10000)
Actual Velocity (Thermal Rayleigh Number (Ra)=100000)
Predicted Velocity (Thermal Rayleigh Number (Ra)=100000)
Velocity
Nanoparticle Concentration (φ)

(b)

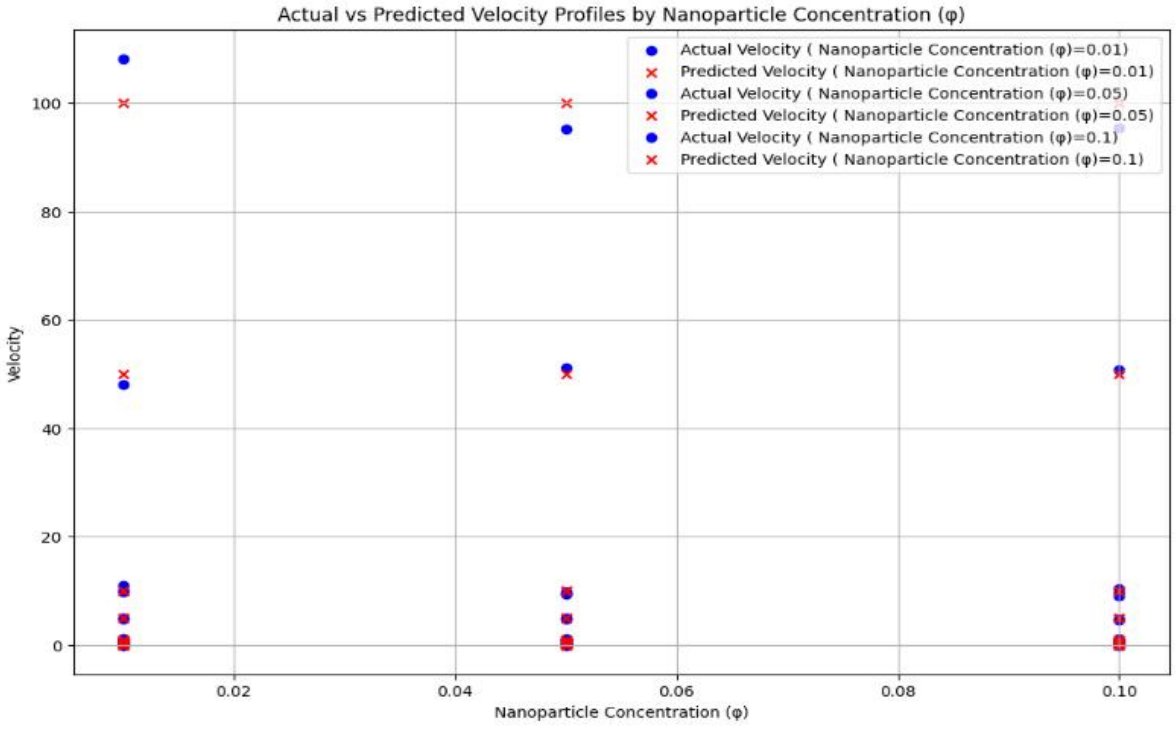
Actual vs Predicted Velocity Profiles by Nanoparticle Concentration (φ)
Actual Velocity (Nanoparticle Concentration (φ)=0.01)
Predicted Velocity (Nanoparticle Concentration (φ)=0.01)
Actual Velocity (Nanoparticle Concentration (φ)=0.05)
Predicted Velocity (Nanoparticle Concentration (φ)=0.05)
Actual Velocity (Nanoparticle Concentration (φ)=0.1)
Predicted Velocity (Nanoparticle Concentration (φ)=0.1)
Velocity
Nanoparticle Concentration (φ)

(c)

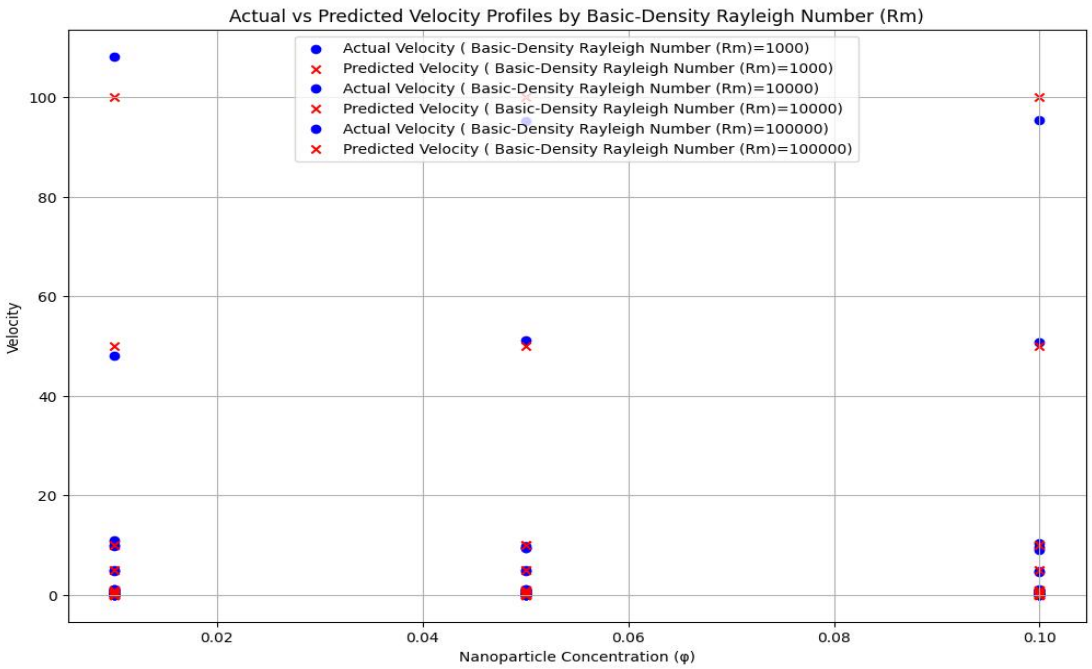

(d)

Figure 10;Actual and predicted velocity (a) AI Model (b) Thermal Rayleigh Number (c)Nanopartical concetration (d)Basic-Density Rayleigh Number.

Table 3: *This table captures the comparison of actual and predicted velocities based on the key parameters of the ferrofluid flow study.*

Index	Thermal Rayleigh Number (Ra)	Ferrohydrodynamic Interaction (β)	Basic-Density Rayleigh Number (Rm)	Nanoparticle Concentration (φ)	Actual Velocity	Predicted Velocity
0	1000	0.1	1000	0.01	0.108124	0.099999
1	1000	0.1	1000	0.05	0.090500	0.099995
2	1000	0.1	1000	0.10	0.107038	0.099990
3	1000	0.1	10000	0.01	0.010119	0.010000
4	1000	0.1	10000	0.05	0.010090	0.010000
...	...	...	...	...	...	...
76	100000	1.0	10000	0.05	9.442662	9.999950
77	100000	1.0	10000	0.10	9.618111	9.999900
78	100000	1.0	100000	0.01	0.912448	1.000000
79	100000	1.0	100000	0.05	0.944153	1.000000
80	100000	1.0	100000	0.10	0.918314	0.999999

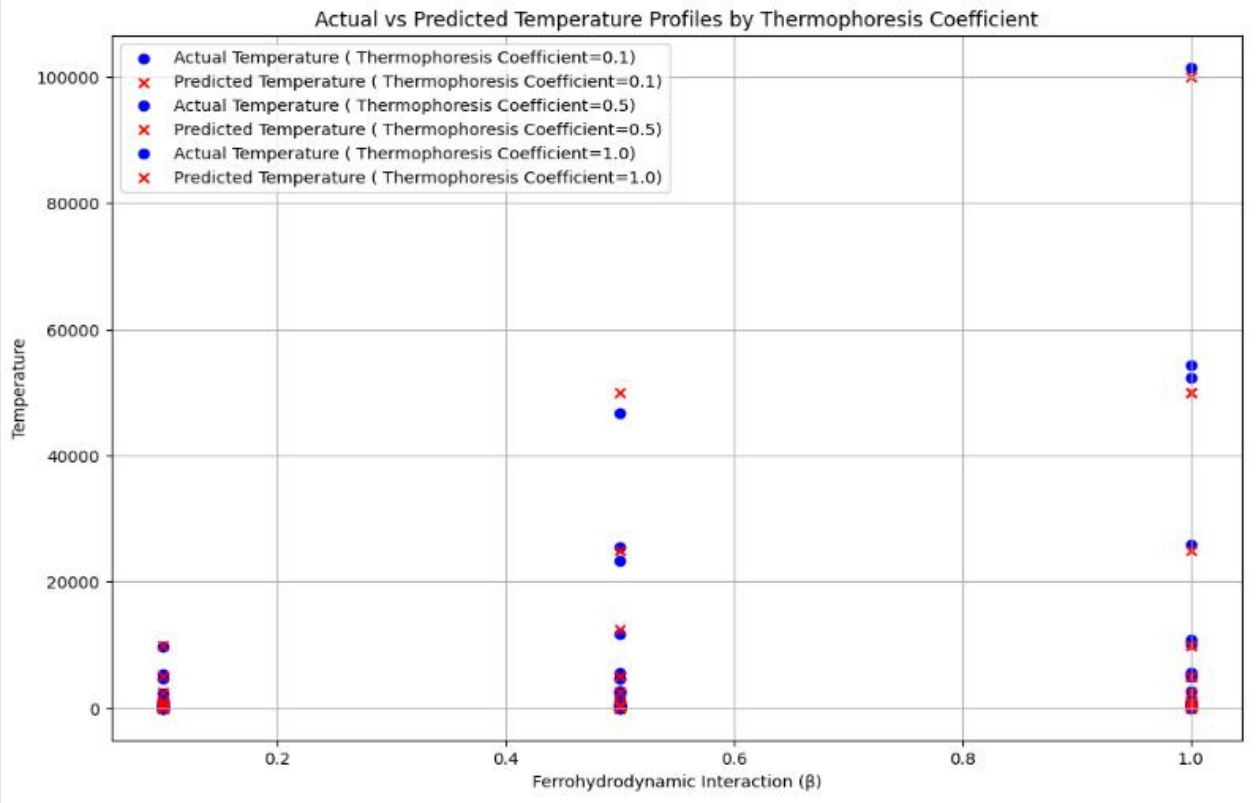

(a)

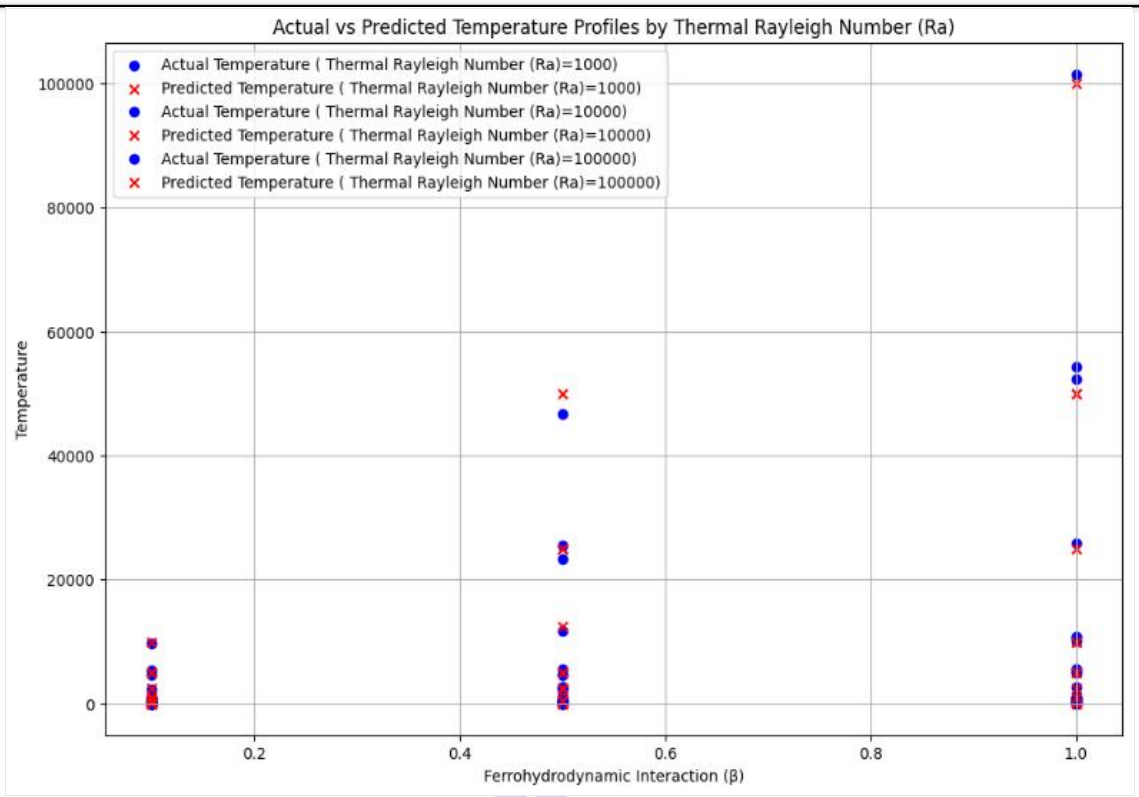

(b)

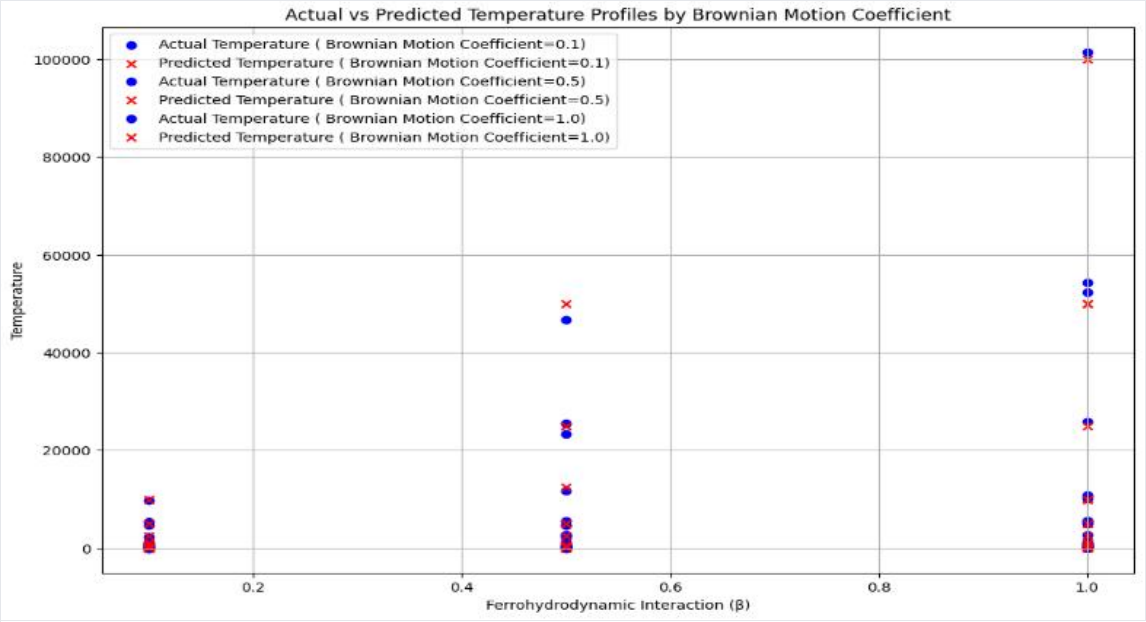

(c)

Figure11; Actual and Predicted Temperatur(a)Thermophorsis coefficient (b)Thermal Rayleigh Number (c) Brownian Motion.

Table 4: This table provides the relationship between thermophoresis coefficient, Brownian motion coefficient, ferrohydrodynamic interaction, and thermal Rayleigh number, along with the corresponding actual and predicted temperature values.

Index	Thermophoresis Coefficient	Brownian Motion Coefficient	Ferrohydrodynamic Interaction (β)	Thermal Rayleigh Number (Ra)	Actual Temperature	Predicted Temperature
0	0.1	0.1	0.1	1000	1.030827	1.0
1	0.1	0.1	0.1	10000	10.306308	10.0
2	0.1	0.1	0.1	100000	90.775250	100.0
3	0.1	0.1	0.5	1000	4.665781	5.0
4	0.1	0.1	0.5	10000	48.520897	50.0
.....						
76	1.0	1.0	0.5	10000	5485.253356	5000.0
77	1.0	1.0	0.5	100000	46613.843105	50000.0
78	1.0	1.0	1.0	1000	962.557387	1000.0
79	1.0	1.0	1.0	10000	10695.465345	10000.0
80	1.0	1.0	1.0	100000	101480.079034	100000.0

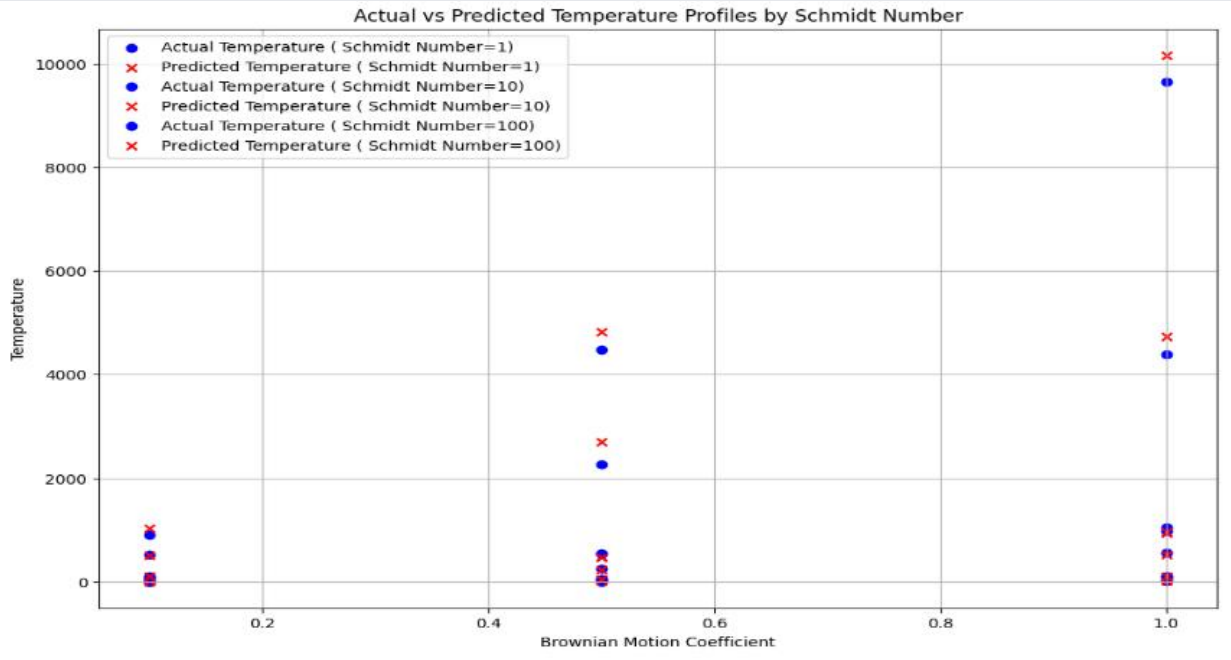

(a)

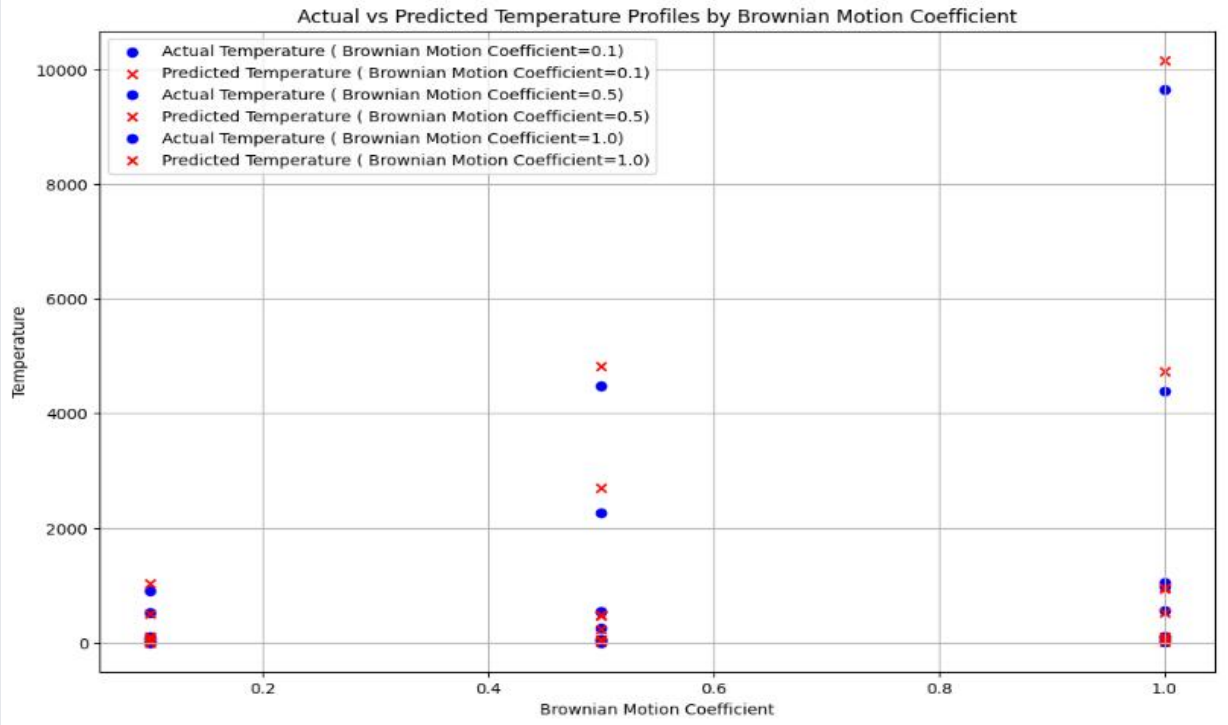

(b)

Figure12; Actual and predicted temperature (a)Schmidt Number (b)Brownian Motion coefficient.

Table 4: This table provides the relationship between thermophoresis coefficient, Brownian motion coefficient along with the corresponding actual and predicted temperature values.

Index	Schmidt Number	Thermophoresis Coefficient	Brownian Motion Coefficient	Actual Temperature	Predicted Temperature
0	1	0.1	0.1	1.10086	1.08599
1	1	0.1	0.5	4.45887	5.47858
2	1	0.1	1	9.3975	9.76303
3	1	0.5	0.1	4.75047	5.23236
4	1	0.5	0.5	25.1548	26.2603
5	1	0.5	1	41.7181	50.526
6	1	1	0.1	9.8124	10.7452
7	1	1	0.5	51.5343	48.5378
8	1	1	1	98.8446	93.5888
9	10	0.1	0.1	9.36789	9.76403
10	10	0.1	0.5	45.2732	49.9859
11	10	0.1	1	102.186	100.586
12	10	0.5	0.1	57.2606	54.1352
13	10	0.5	0.5	247.809	230.715
14	10	0.5	1	555.699	526.337

15	10	1	0.1	85.1499	107.536
16	10	1	0.5	532.145	492.674
17	10	1	1	1055.06	940.507
18	100	0.1	0.1	98.281	104.96
19	100	0.1	0.5	537.55	466.91
20	100	0.1	1	974.161	961.723
21	100	0.5	0.1	531.175	498.303
22	100	0.5	0.5	2260.48	2703.21
23	100	0.5	1	4379.07	4737.3
24	100	1	0.1	895.778	1022.72
25	100	1	0.5	4472.72	4830.83
26	100	1	1	9647.58	10161.5

Physics-Informed NeuralNetwork (PINN) Development:

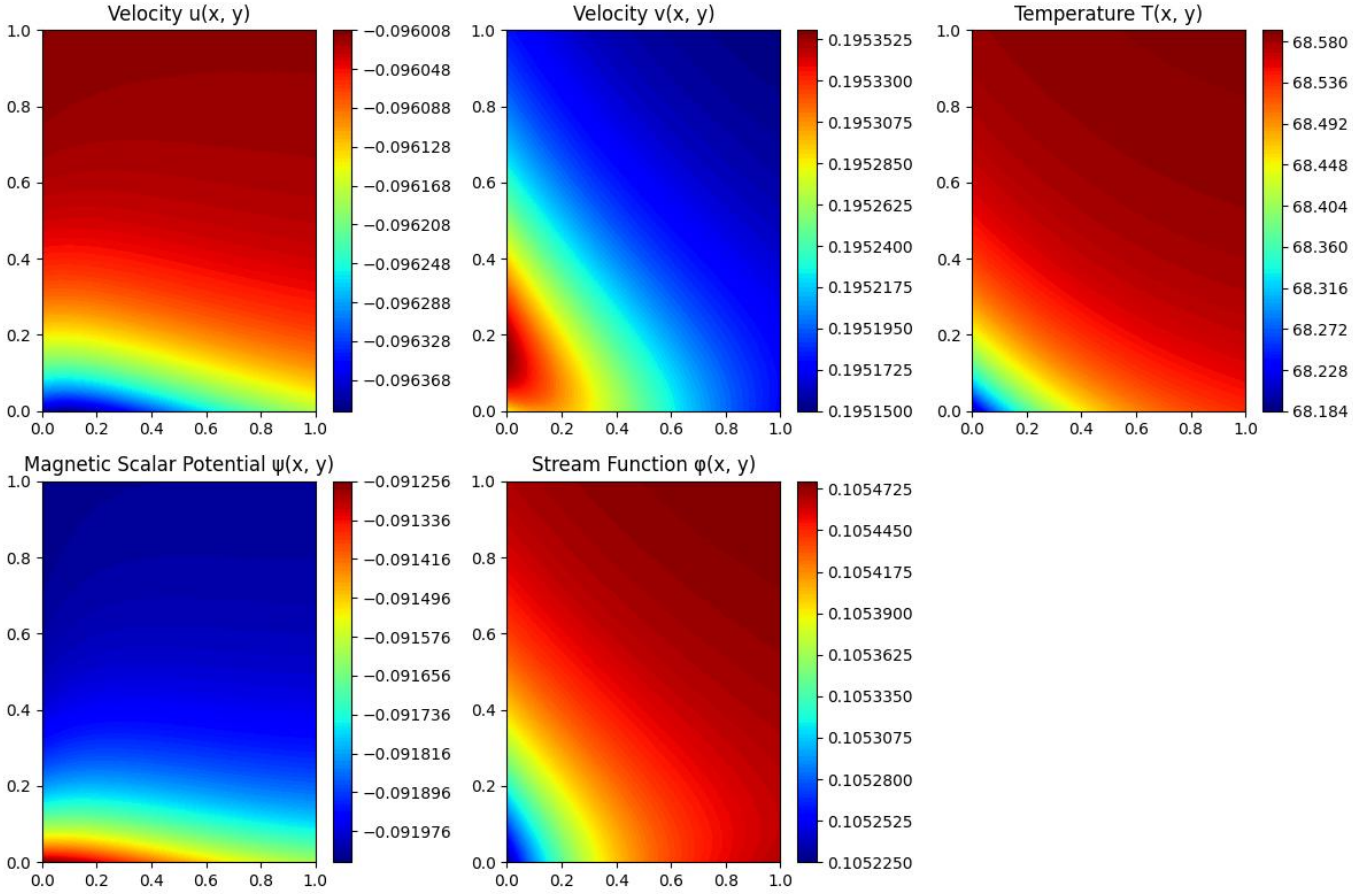

Figure13; Physics-Informed NeuralNetwork on velocity,Temperature,Magnetic Scalar,Stream Function.

Index	x	y	u(x, y)	v(x, y)	T(x, y)	ψ(x, y)	φ(x, y)
0	0.25	0.25	-0.096104	0.195259	68.528755	-0.091860	0.105411
1	0.50	.50	-0.096032	0.195181	68.577415	-0.091982	0.105462

2	0.75	0.75	-0.096018	0.195158	68.586639	-0.092014		0.105474

Random Forest Model:

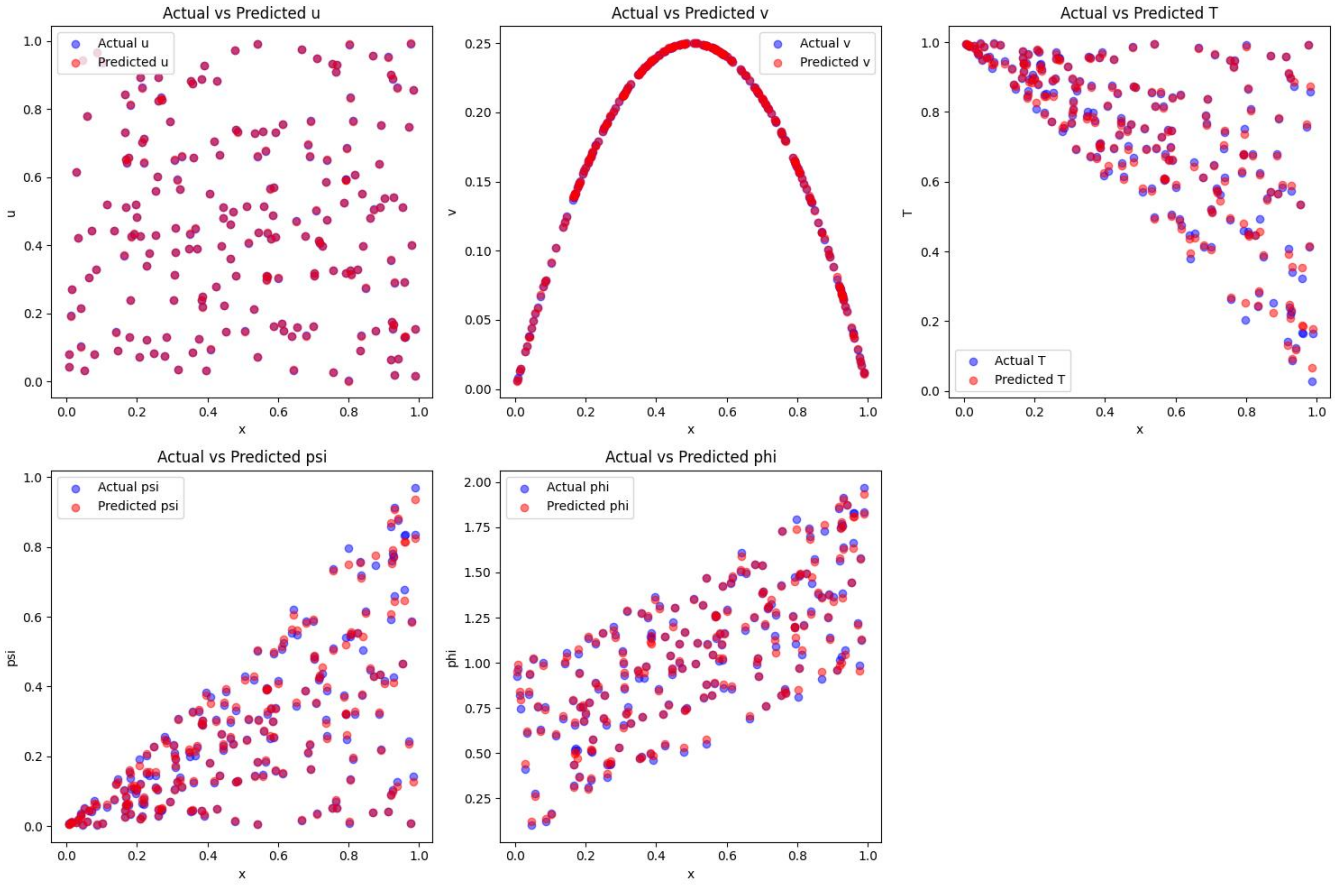

Index	Actual u	Predicted u	Actual v	Predicted v	Actual T	Predicted T	Actual ψ	Predicted ψ	Actual φ	Predicted φ
521	0.22435	0.22279	0.24727	0.24737	0.65271	0.64659	0.34729	0.35364	1.22339	1.2002
737	0.75587	0.75642	0.23735	0.23734	0.85048	0.847	0.14952	0.15322	0.8566	0.87069
740	0.67617	0.67903	0.24588	0.24593	0.81729	0.8118	0.18271	0.18848	0.88804	0.89237
660	0.28967	0.29264	0.06559	0.06469	0.33979	0.35574	0.66021	0.64326	1.63977	1.63119
411	0.95673	0.9561	0.11357	0.1131	0.96238	0.96044	0.03762	0.03953	0.91264	0.94829

6. Conclusion and Future Recommendation

This study explores the dynamics of ferrofluids, with a particular focus on how temperature stratification influences the flow behavior of ferrofluids over a flexible surface when exposed to a magnetic dipole. Several key findings emerged from our analysis;

- With the increase in the ferromagnetic interaction parameter, there is a clear improvement in the heat transfer. The improvement is, however, associated with a decrease in the axial velocity of the fluid, thus revealing the relationship between heat transfer efficiency and fluid motion.
- Increased thermal stratification parameter (S) results in narrower velocity and temperature fields. Interestingly, the more value of S, the more enhanced the heat transfer, indicating that the temperature gradients are also important in improving the heat transfer.
- The ratio parameter (R) has a direct effect on axial velocity. Thus, with increasing value of R, the axial velocity also increases which shows how significant it is in controlling the behavior of the fluid flow.
- The Prandtl number influences the temperature field by diminishing the temperature field but with interesting property, it enhances the local Nusselt number (the efficiency of convective heat transfer).
- The Physics-Informed Neural Network (PINN) model and the Random Forest model were used to predict the flow and thermal response of ferrofluids. The two advanced machine learning models that were used for the prediction of the flow and thermal response of ferrofluids were the Physics-Informed Neural Network (PINN) model and the Random Forest model. The results of both models showed good predictive capability and good agreement between the measured and predicted velocity and temperature distribution. The PINN model, which incorporates the physical laws directly to the learning process, gave a slightly better prediction, especially for temperature. However, the Random Forest model was more efficient in computation, but achieved comparable accuracy in most parameters, making it a good alternative for applications where speed is the major concern.
- This study contributes to the understanding of the control of the ferrofluid flow and heat transfer in practical use. The physics-based models combined with machine learning provide valuable insights into optimizing ferrofluid behavior for different engineering applications. Additional research could build upon these findings to better understand how other parameters affect ferrofluid behavior, and thereby create even more precise models for predicting ferrofluid behavior. These developments will help to make better use of the ferrofluid in systems, from thermal applications to fluid manipulation and control, more efficient.

References

1. Khelfallah, M., et al., *Structural and Magnetic Properties of Ferrofluids Composed of Self-Assembled Cobalt Ferrite Nanoflowers: A Multiscale Investigation.* The Journal of Physical Chemistry C, 2024. **128**(31): p. 13162-13176.
2. Mehrez, Z., *Heat transfer enhancement with ferrofluids*, in *Advanced Materials-Based Fluids for Thermal Systems*. 2024, Elsevier. p. 61-100.
3. Ryapolov, P., et al., *Magnetic fluids: The interaction between the microstructure, macroscopic properties, and dynamics under different combinations of external influences.* Nanomaterials, 2024. **14**(2): p. 222.
4. Sreelakshmi, T., et al., *Nonlinear thermal buoyancy on ferromagnetic liquid stream over a radiated elastic surface with non fourier heat flux.* Computer Modeling in Engineering & Sciences, 2021. **126**(2): p. 599-616.
5. Patel, H., et al., *Optimized Mn0. 5Zn0. 5Fe2O4 nanoflowers based magnetic fluids for potential biomedical applications.* Journal of Magnetism and Magnetic Materials, 2024. **590**: p. 171656.
6. Cardoso, V.F., et al., *Advances in magnetic nanoparticles for biomedical applications.*

Advanced healthcare materials, 2018. 7(5): p. 1700845.
7. Nikolic, M., *Magnetic Spinel Ferrite Nanoparticles: From Synthesis to Biomedical Applications.* Magnetic Nanoparticles for Biomedical Applications, 2023. 143: p. 41-75.
8. Ossege, F., R. Gontijo, and A. de Paula, *Dynamical analysis of a ferrofluid subjected to oscillatory field and shear rates: Applications to magnetic hyperthermia.* Journal of Magnetism and Magnetic Materials, 2024. 596: p. 171936.
9. Deebani, W., et al., *Numerical simulation and stability analysis of radiative magnetized hybridized ferrofluid flow with acute magnetic force over shrinking/stretching surface.* Results in Engineering, 2024. 22: p. 102315.
10. Yasin, S.H.M., et al., *Flow and Heat Transfer of Micropolar Ferrofluid at Stagnation Point on a Horizontal Flat Plate in the Presence of Magnetic Field and Thermal Radiation.* Journal of Advanced Research in Fluid Mechanics and Thermal Sciences, 2023. 110(1): p. 227-238.
11. Abbas, K., et al., *Recent developments in the application of ferrofluids with an emphasis on thermal performance and energy harvesting.* Journal of Magnetism and Magnetic Materials, 2023: p. 171311.
12. Iftikhar, B., M.A. Siddiqui, and T. Javed, *Dynamics of magnetohydrodynamic and ferrohydrodynamic natural convection flow of ferrofluid inside an enclosure under non-uniform magnetic field.* Alexandria Engineering Journal, 2023. 66: p. 523-536.
13. Khan, A., et al., *Hydrodynamic analysis of the magnetic field dependent viscous fluid flow and thermosolutal convection between rotating channels.* Scientific Reports, 2022. 12(1): p. 17170.
14. Oyelami, F.H., et al., *Magneto-Hemodynamics Fluid Hyperthermia in a Tumor with Blood Perfusion.* Mathematical Modelling of Engineering Problems, 2022. 9(5).
15. Tabrez, M., et al., *Dynamics of ferromagnetic cross fluid flow capturing magnetic dipole and radiation aspects.* Modern Physics Letters B, 2024. 38(16): p. 2341006.
16. Sarif, N.M., M.Z. Salleh, and R. Nazar, *Numerical solution of flow and heat transfer over a stretching sheet with Newtonian heating using the Keller box method.* Procedia Engineering, 2013. 53: p. 542-554.
17. Kameswaran, P., et al., *Homogeneous–heterogeneous reactions in a nanofluid flow due to a porous stretching sheet.* International journal of heat and mass transfer, 2013. 57(2): p. 465-472.
18. Abbas, Z., M. Sheikh, and I. Pop, *Stagnation-point flow of a hydromagnetic viscous fluid over stretching/shrinking sheet with generalized slip condition in the presence of homogeneous–heterogeneous reactions.* Journal of the Taiwan Institute of Chemical Engineers, 2015. 55: p. 69-75.
19. Malik, M., et al., *Homogeneous-heterogeneous reactions in Williamson fluid model over a stretching cylinder by using Keller box method.* AIP Advances, 2015. 5(10).
20. Khan, I., et al., *Homogenous–heterogeneous reactions in MHD flow of Powell–Eyring fluid over a stretching sheet with Newtonian heating.* Neural Computing and Applications, 2018. 30: p. 3581-3588.
21. Toscano, J.D., et al., *From PINNs to PIKANs: Recent Advances in Physics-Informed Machine Learning.* arXiv preprint arXiv:2410.13228, 2024.
22. Zhang, W., et al., *A General Method for Solving Differential Equations of Motion Using Physics-Informed Neural Networks.* Applied Sciences, 2024. 14(17): p. 7694.
23. Park, N., et al. *Parameterized Physics-informed Neural Networks for Parameterized PDEs*. in *International Conference on Machine Learning (ICML 2024)*. 2024. ICML.
24. Hao, J., et al. *Improving Information Propagation of Physics-Informed Neural Networks with General Causality Principle*. in *2024 6th International Conference on Data-*

driven Optimization of Complex Systems (DOCS). 2024. IEEE.
25. Cao, Y., et al. *System stabilization of pdes using physics-informed neural networks (pinns)*. in *2024 43rd Chinese Control Conference (CCC)*. 2024. IEEE.
26. Sikora, M., et al., *Comparison of Physics Informed Neural Networks and Finite Element Method Solvers for advection-dominated diffusion problems.* Journal of Computational Science, 2024: p. 102340.
27. Garay, J., et al., *Physics-informed neural networks for parameter estimation in blood flow models.* Computers in Biology and Medicine, 2024: p. 108706.
28. Titus, L.R. and A. Abraham, *Heat transfer in ferrofluid flow over a stretching sheet with radiation.* International Journal of Engineering Research and Technology, 2014. **3**(6): p. 2198-2203.
29. Majeed, A., A. Zeeshan, and R. Ellahi, *Unsteady ferromagnetic liquid flow and heat transfer analysis over a stretching sheet with the effect of dipole and prescribed heat flux.* Journal of Molecular liquids, 2016. **223**: p. 528-533.
30. Hayat, T., et al., *Entropy generation optimization of MHD Jeffrey nanofluid past a stretchable sheet with activation energy and non-linear thermal radiation.* Physica A: Statistical Mechanics and its Applications, 2020. **544**: p. 123437.
31. Reddy, A.S., et al., *MHD flow of non-Newtonian ferro nanofluid between two vertical porous walls with Cattaneo–Christov heat flux, entropy generation, and time-dependent pressure gradient.* Nonlinear Analysis: Modelling and Control, 2023. **28**(4): p. 655-671.
32. Kumar, P., et al., *Revolutionizing Heat Transfer and Fluid Flow Models: Fractional Calculus and Non-Newtonian Dynamics Meet Advanced Numerical Methods.* Journal of Computational Analysis and Applications (JoCAAA), 2024. **33**(06): p. 375-387.
33. Alizadeh, R., et al., *A machine learning approach to predicting the heat convection and thermodynamics of an external flow of hybrid nanofluid.* Journal of Energy Resources Technology, 2021. **143**(7): p. 070908.
34. Saha, A., A. Basu, and S. Banerjee, *Enhancing thermal management systems: a machine learning and metaheuristic approach for predicting thermophysical properties of nanofluids.* Engineering Research Express, 2024. **6**(4): p.
35. Petrini, P.A., D. Lester, and G. Rosengarten, *Enhanced laminar heat transfer via magnetically driven ferrofluids.* International Journal of Heat and Mass Transfer, 2023. **217**: p. 124703.
36. Banerjee, S., *Basics and applications of ferrofluids*, in *Handbook of Research on Developments and Trends in Industrial and Materials Engineering*. 2020, IGI Global. p. 366-400.
37. Anjum Jumana, S., et al., *Flow of a biomagnetic fluid embedded by magnetic dipole over a continuously moving sheet.* ZAMM-Journal of Applied Mathematics and Mechanics/Zeitschrift für Angewandte Mathematik und Mechanik, 2024: p. e202100203.
38. PArmAr, A. and S. Jain, *Comparative study of flow and heat transfer behavior of Newtonian and non-Newtonian fluids over a permeable stretching surface.* Global and Stochastic analysis, 2017. **25**(1): p. 41-50.
39. Zhao, Q., H. Xu, and T. Fan, *Analysis of three-dimensional boundary-layer nanofluid flow and heat transfer over a stretching surface by means of the homotopy analysis method.* Boundary Value Problems, 2015. **2015**: p. 1-18.
40. Chouhan, K.K. and S. Chaudhary, *Hybrid ferrofluid flow on a stretching sheet with Stefan blowing and magnetic polarization effects in a porous medium.* Multidiscipline Modeling in Materials and Structures, 2024. **20**(6): p. 1013-1037.
41. Williams, G.P., *Numerical integration of the three-dimensional Navier-Stokes equations for*

incompressible flow. Journal of Fluid Mechanics, 1969. **37**(4): p. 727-750.
42. !!! INVALID CITATION !!! .
43. Batiha, B., *Innovative Solutions for the Kadomtsev–Petviashvili Equation via the New Iterative Method.* Mathematical Problems in Engineering, 2024. **2024**(1): p. 5541845.
44. Das, P.K., *A review based on the effect and mechanism of thermal conductivity of normal nanofluids and hybrid nanofluids.* Journal of Molecular Liquids, 2017. **240**: p. 420-446.
45. Cuomo, S., et al., *Scientific machine learning through physics–informed neural networks: Where we are and what's next.* Journal of Scientific Computing, 2022. **92**(3): p. 88.
46. Biau, G., *Analysis of a random forests model.* The Journal of Machine Learning Research, 2012. **13**(1): p. 1063-1095.
47. Shaik, A.B. and S. Srinivasan. *A brief survey on random forest ensembles in classification model.* in *International Conference on Innovative Computing and Communications: Proceedings of ICICC 2018, Volume 2*. 2019. Springer.